CRYPTOCHROME suppresses the circadian proteome and promotes protein homeostasis

Authors

David C.S. Wong[1], Estere Seinkmane[1], Alessandra Stangherlin[1], Aiwei Zeng[1], Nina M. Rzechorzek[1], Andrew D. Beale[1], Jason Day[2], Martin Reed[1], Sew Peak Chew[1], Christine T. Styles[3], Rachel S. Edgar[3], Marrit Putker[1,4] & John S. O'Neill*[1].

Affiliations

[1]MRC Laboratory of Molecular Biology, Cambridge, UK.

[2]Department of Earth Sciences, University of Cambridge, Cambridge, UK.

[3]Department of Infectious Diseases, Imperial College, London, UK.

[4]Current address: Crown Bioscience, Utrecht, the Netherlands.

*Correspondence to: oneillj@mrc-lmb.cam.ac.uk

Abstract

The daily organisation of most mammalian cellular functions is attributed to circadian regulation of clock-controlled protein expression, driven by daily cycles of CRYPTOCHROME-dependent transcriptional feedback repression. To test this, we compared the circadian proteome and phosphoproteome of wild type and CRY-deficient fibroblast cells. Strikingly, CRY-deficient cells showed a two-fold increase in circadian-regulated proteins, phosphopeptides, and K^+ transport. This was accompanied by extensive remodelling of the cellular proteome overall, including reduced phosphatase and proteasome subunit expression. These adaptations rendered CRY-deficient cells more sensitive to stress, which may account for their reduced circadian robustness and contribute to the wide-ranging phenotypes of CRY-deficient mice. We suggest that CRY ultimately functions to suppress, rather than generate, daily rhythms in cellular protein abundance, thereby maintaining protein and osmotic homeostasis.

Introduction

From transcriptional activation and RNA processing, to protein synthesis, folding and degradation, multiple mechanisms operate at every stage of gene expression to ensure that each cellular protein is maintained in a concentration range appropriate to its biological function [1–3]. Proteome homeostasis is essential for cell viability and osmotic homeostasis, with the correct temporal regulation of protein activity being critical to every biological process—too much or too little at the wrong time underlies most pathological states [4,5].

In mammals, cellular physiology is temporally orchestrated around daily cycles that regulate most biological functions and much of the proteome to a circadian rhythm, whereas circadian dysregulation is strongly associated with pathological states [6]. On any given day, the circadian cycle is expressed by more cells of the human body than the cell division cycle, with daily rhythms in clock-controlled protein abundance thought to be the fundamental basis by which cell biology anticipates and accommodates the predictable demands of day and night [6,7]. Individual cellular rhythms are synchronised by endocrine cues such as insulin and glucocorticoid signalling, which function *in vivo* to align internal cellular timing with environmental cycles [8]. Daily rhythms in proteome composition are readily observed *in vivo* and persist in cultured cells under constant conditions *ex vivo* [9,10]. The average daily variation of rhythmically abundant proteins across a range of cellular contexts is ~10-20% [9–12]. There is little direct evidence that such modest variation would necessarily elicit rhythms in protein function, however, given that protein abundance is rarely rate-limiting for protein activity under physiological conditions [13–16].

Circadian regulation of a protein's abundance is most frequently attributed to cycling transcription of the encoding gene, despite recent investigations having revealed that mRNA and protein abundances correlate quite poorly, and that post-transcriptional and post-translational regulatory processes are at least as important [17–21]. Global transcriptional oscillations are facilitated by daily cycles of

transcriptional repression and derepression effected by products of the *Period1/2* and *Cryptochrome1/2* genes, and fine-tuned by various auxiliary but non-essential transcriptional feedback mechanisms [17,18]. The transcription of *Period*, *Cryptochrome* and other genes is stimulated by complexes containing the activating transcription factor BMAL1. The stability, interactions, and nucleocytoplasmic shuttling of the encoded PER and CRY proteins is regulated post-translationally until, many hours later, they repress the activity of BMAL1-containing complexes in a transcriptional-translation feedback loop (TTFL).

Within the TTFL circuit, CRY proteins are the essential repressors of BMAL1 complex activity [22,23], whereas, PER proteins play critical signalling and scaffolding roles, required for the nuclear import and targeting of CRY to BMAL1-containing complexes [23]. CRY proteins also function as adaptors for the recruitment of E3 ubiquitin ligase complexes that target many proteins, including transcription factors, for ubiquitin-mediated proteolysis [24]. According to the current widely-accepted paradigm therefore, CRY-mediated transcriptional feedback repression is indispensable for the cell-autonomous circadian regulation of gene expression [25–29], with resultant rhythms in clock-controlled protein abundance driving the daily co-ordination of cellular activity [30].

Critically though, CRY-deficient cells and tissues remain competent to sustain circadian timing in the absence of TTFL function [31–33], with a mechanism that is dependent on casein kinase 1 and protein degradation, as in wild type controls, as well as in naturally anucleate red blood cells [34–36]. Similarly, circadian oscillations persist in cells and tissue slices lacking BMAL1 [37,38]. Since BMAL1 and CRY proteins are required for normal circadian regulation *in vivo*, and also required for TTFL function, it was thought that the complex phenotype of BMAL1- or CRY-deficient mice arises because circadian timekeeping is crucial for cellular and organismal physiology more generally [39,40]. The emerging observation that BMAL1 and CRY-deficient cells and tissues are competent to sustain certain elements of circadian regulation challenges this interpretation and suggests an alternative hypothesis:

that some or all phenotypic complexity associated with deletion of a 'clock gene' arises from additional functions of the encoded protein beyond the canonical TTFL model. Supporting this, several recent reports imply that various pathophysiological consequences of CRY-deficiency might be directly attributable to the absence of CRY function rather than impairment of circadian transcriptional regulation [12,41–44]. Overall then, current evidence suggests that whilst CRY-mediated circadian transcriptional feedback repression is crucial for cycling TTFL activity, rhythmic robustness and co-ordinating outputs [7,23,26,28,29,36], it is not essential for the cell-intrinsic capacity to maintain daily timekeeping [33].

To test this alternative hypothesis, and thereby gain insight into how CRY confers rhythmic robustness, we investigated the molecular consequences of CRY deficiency on cellular protein expression over several days using an unbiased whole cell (phospho)proteomic strategy. Our findings reveal a crucial role for CRY in the maintenance of protein and osmotic homeostasis, with CRY-deficient cells exhibiting a chronic stress-like state that may underlie their reduced robustness as well as the complex and numerous consequences of CRY deletion in mice and their tissues.

Results

Cell-autonomous rhythms in the proteome and phosphoproteome persist in the absence of CRY

To understand the proteomic and phosphoproteomic consequences of CRY deletion, we used confluent primary mouse fibroblasts, a classic model of cellular circadian timekeeping where contact inhibition prevents any interference from the cell division cycle [9]. Wild-type (WT) and CRY1$^{-/-}$; CRY2$^{-/-}$ (CKO) mouse fibroblasts in cell culture were isolated from otherwise isogenic mice and synchronised using daily temperature cycles then sampled under constant conditions (Figure 1A). Quantitative proteomics detected over 6000 proteins and around 4000 phosphopeptides in both cell types. We were surprised to find that, averaging across the time course, the overall abundance and relative phosphorylation of most detected proteins was significantly altered in CKO cells compared with WT controls (Figure 1B, C), by an average of 21%. This striking CRY-dependent change in overall proteome composition was similar to previous findings in CKO mouse liver [12] (Figure S1A).

In our cellular time course, as expected [26,28,45], CRY1 was selectively detected in WT, but not CKO cells, and displayed a ~24h rhythmic abundance profile across the time course with delayed phase relative to a PER2 luciferase reporter (PER2::LUC) recorded from parallel replicate cultures (Figure S1B). Heatmaps visualising the rhythmic proteins are shown in Figure S1D/E; with examples of rhythmic and arrhythmic (phospho)proteins shown in Figure S1F/G. Based on estimates of intrinsic noise of gene expression [46–50], we chose a threshold of 10% relative amplitude to define biological significance for protein abundance oscillations; no such studies were available for protein phosphorylation.

In WT cells, 7% of detected proteins and 8% of detected phosphopeptides showed significant circadian abundance rhythms. Unexpectedly, 17% of detected proteins and 14% of phosphopeptides in CKO cells were rhythmically abundant (Figure 1D, E). Using an independent statistical tool to test

for rhythmicity (eJTK cycle), we found that similarly, more rhythmic species were present in CKO cells compared with WT, and with small overlap (Figure S1C).

CRY suppresses the cell-autonomous rhythmic proteome and phosphoproteome

Amongst the minority of proteins that were rhythmically abundant in both genotypes (Figure 1D), there was a modest but significant increase of median relative amplitude in CKO cells compared with WT (Figure 2A). We calculated the mean abundance of each detected protein over time and divided them into deciles of abundance. We then plotted the proportion of proteins within each decile that were rhythmic against the abundance mid-point of each decile. In this way we found that more abundant proteins were more likely to be rhythmic than less abundant proteins, but crucially, this relationship was stronger for CKO cells compared to WT cells (Figure 2B). Although part of this correlation may be due to preferential and more accurate detection of oscillating high abundance proteins, this explanation cannot account for the different relationships in WT and CKO cells. As with proteins, we found that CKO rhythmic phosphopeptides were significantly increased in relative amplitude and abundance compared with WT (Figure 2C, D). Therefore, the TTFL-independent circadian rhythm seen in CKO cells drives oscillations of higher relative amplitude and acts preferentially towards more abundant proteins and phosphopeptides.

The phase distribution of rhythmic proteins in both genotypes was clustered at experimental time 0 h (Figure 2E, F), when PER2::LUC activity in wild type cells was maximal (Figure S1A). This phase clustering was also true for proteins that were only rhythmic in CKO cells (Figure 2H), and for most proteins that were only rhythmic in WT cells (Figure 2G). A subset of proteins and phosphopeptides that were rhythmic in WT only, including CRY1, were clustered at a later circadian phase (Figure 2G). This cluster was not present in proteins and phosphopeptides that were rhythmic in CKO only (Figure 2H). In WT cells we observed clustering of protein phosphorylation to an earlier phase (by 3 h) compared to rhythmically abundant proteins and PER2::LUC (Figure 2I) with higher relative

147 amplitude (Figure 1E); this phase relationship has strong similarities with observations in mouse liver
148 *in vivo* [51]. Whilst the same was true for CKO cells, there was a much broader distribution of phase
149 among rhythmic phosphopeptides across 9 h that preceded peak rhythmic protein abundance (Figure
150 2J).
151
152 These observations demonstrate that cell-autonomous rhythmic regulation of protein abundance and
153 phosphorylation occurs independently of CRY. Instead, the primary role of CRY appears to be two-
154 fold. First, consistent with its function as a rhythmic repressor of gene expression, CRY suppresses
155 the amplitude of cellular protein and phosphopeptide abundance rhythms. Greater amplitudes were
156 observed in the absence of CRY, coupled with more than twice the number of rhythmic proteins
157 detected in WT cells, and with most rhythmic CKO (phospho)proteins not being detectably rhythmic
158 in WT cells (Figure 1D, E). Secondly, in WT cells, CRY regulates the phase of rhythmicity for a sub-
159 population of proteins and phosphopeptides whose abundance peaks around the same phase as CRY1
160 and in antiphase with the majority of the rhythmic (phospho)proteome.
161
162 Overall, we observed that a remarkable 82% of detected proteins in CKO cells were altered in
163 abundance compared with WT (Figure S2A, Abundance up + down), suggesting that the respective
164 synthesis and degradation rates of many proteins are altered by CRY deficiency. We postulated that
165 CRY deletion might unmask rhythmicity in proteins that normally exhibit matched rhythms of
166 synthesis and degradation in WT cells, i.e. constitutively present with rhythmic turnover. Supporting
167 this, there was a significant association between changes in average protein abundance and changes
168 in rhythmicity: we found that proteins that changed in overall abundance were more likely to change
169 in rhythmicity: from arrhythmic to become rhythmic, or *vice versa* (Figure S2A). In this case, our
170 observations would indicate that the cell-autonomous circadian clock regulates ~ 30% of the
171 fibroblast proteome (Figure S2A, green + blue + brown), with CRY primarily acting to suppress
172 rhythms in the abundance of most of these proteins (Figure S2A, green).

In fact, we found that there was greater overall variation in abundance of proteins detected in CKO cells (Figure S2B), suggesting that CRY may suppress changes in protein levels more generally. To verify this finding using an independent dataset, we calculated the fold-change in abundance for proteins detected by Mauvoisin *et al*. from WT and CKO mouse liver samples [12]. There was greater variation in protein abundance in CKO compared with WT (Figure S2C). Therefore, CRY also functions to suppress variation in protein abundance in mouse liver *in vivo* under diurnal conditions.

To test the effects of CRY deletion on the phosphoproteome, we performed the same analysis with detected phosphopeptides. As with the proteome, we found a strong link between changes in abundance and rhythmicity of phosphopeptides between the two genotypes (Figure S2D), as well as greater variation in phosphopeptide abundance in CKO compared with WT cells (Figure S2E).

We also observed an increase in overall protein phosphorylation in CKO cells (Figure 1C, S3A). We therefore considered whether CRY deletion might impact upon the abundance or activity of protein kinases and phosphatases, which act in dynamic equilibrium to determine the phosphorylation level of each peptide we detected. In our proteomics dataset there was no significant overall change in abundance of protein kinases (Figure S3B). To validate this, we employed the PHOSIDA database [52,53] to infer rhythmic kinase activity; and found that targets of kinases typically associated with circadian regulation were not over-represented in WT or CKO rhythmic datasets compared to background, nor in the set of phosphopeptides that were rhythmic in both genotypes (Figure S3C-E). CKO cells did show an overall decrease in abundance of protein phosphatases however (Figure S3B), which may plausibly account for both increased overall phosphorylation and increased rhythmic phosphorylation in CKO compared with WT cells. This would suggest that CRY normally functions to globally supress steady-state protein phosphorylation, as well as rhythms in protein phosphorylation, in part through regulation of phosphatase abundance.

Bringing these observations together we suggest that the synthesis and degradation of many proteins, as well as the phosphorylation and dephosphorylation of many phosphosites, may be coupled through a mechanism that requires CRY to be present. CRY deletion therefore elicits a significant change in dynamic steady-state abundance for most of the (phospho)proteome, including a sub-set of proteins that are normally circadian-regulated, thereby revealing more than twice the number of rhythmic proteins and phosphopeptides detected in WT cells. The altered protein stoichiometries of CKO compared with WT cells and tissues would be described as a state of proteome imbalance if it occurred in the context of cancer cells [54] and is normally associated with altered protein homeostasis. That such proteome imbalance is observed in primary cells and tissues suggests the presence of widespread changes in the cellular determinants of proteome composition [4,5].

CRYPTOCHROME regulates proteasome activity and translation rate

We explored potential mechanisms for the widespread proteome changes in CKO cells by searching our dataset for key factors regulating protein synthesis and degradation. We did not interrogate the transcriptome of CKO cells, which has been adequately addressed elsewhere, and since there is now overwhelming consensus that mRNA abundance is poorly predictive of protein abundance [10–12,55–64]. We found a striking reduction in the abundance of catalytic proteasomal subunits (Figure 3A) which we validated by western blot and enzymatic assays of proteasome activity (Figure 3B-D, S4A).

Whilst there was no consistent change in ribosomal subunit abundance, we also observed a significant increase in cytosolic protein synthesis rate by ^{35}S-methionine incorporation (Figure 3E, S4B, C), as observed previously by puromycin incorporation [33]. We considered that the combined effect of reduced proteasomal activity and increased translation rate would affect the overall steady state levels of cellular protein. We found this to be the case, with a modest but significant increase in overall protein per CKO cell compared with WT (Figure 3F).

These cultured CKO cells express more protein than WT cells, with increased translation and decreased proteasomal degradation. Altogether, and in light of previous observations [65–67], our data suggest that CKO cells likely maintain a different set point for protein homeostasis, as also occurs in many pathological states [4,5].

Rhythmic regulation of ion transport and protein content is CRY-independent

Mammalian and other eukaryotic cells devote significant resources to ensuring osmotic equilibrium over the plasma membrane, in order to maintain cell volume and prevent protein aggregation [67–70]. Changes in cytosolic macromolecule content are balanced by compensatory ion transport, primarily mediated by K^+, the major cellular osmolyte [67,68]. Two independent lines of evidence suggested that CKO cells would exhibit altered osmotic homeostasis.

First, we searched for rhythmically regulated cellular processes in CKO and WT cells using gene ontology (GO) analysis. Of the rhythmically abundant proteins, ranked GO analysis revealed consistent enrichment for processes associated with ion transport, both in wild type and CKO cells when analysed separately or combined (Figure 4A-C). Interrogation of the proteomics dataset then revealed altered expression levels and increased rhythmic amplitudes of many ion transporters in CKO compared with WT cells (Figure S5A, B). This included several members of the SLC12A family of electroneutral transporters (Figure 4F), that contribute to the maintenance of osmotic homeostasis against variations in cytosolic protein concentration in wild type cells over the circadian cycle [71]. Second, since many proteins are cytoplasmic, we considered that if CRY normally suppresses rhythms in the abundance of many individual proteins that normally peak around the same circadian phase (Figure 2E-H) then the consequence of CRY deletion would be to increase the overall amplitude of daily rhythms in soluble cytosolic protein content.

To validate this, we measured the K^+ content of cells across the circadian cycle. Consistent with previous investigations [71], in WT cells, K^+ and digitonin-extracted cytosolic protein concentrations exhibited antiphasic circadian rhythms (Figure 4D, Figure S5C), with no significant daily variation in total cellular protein. The same was observed in CKO cells (Figure 4E), but with higher relative amplitudes for soluble protein and K^+ (Figure 4G, H). Considering previous observations [71], the higher amplitude cytosolic protein rhythm in CKO cells likely drives the higher amplitude K^+ rhythms. This is facilitated by increased expression and amplitude of SLC12A transporter activity (Figure 4F), which buffers cellular osmotic potential in response to greater changes in cytosolic macromolecular content over the circadian cycle [71].

Previous work has suggested that compensatory K^+ transport is a fundamental feature of eukaryotic cell biology allowing cells to accommodate changes in cytosolic macromolecular content whilst maintaining osmotic homeostasis [67,71]. Our present observations suggest that this occurs independently of CRY-mediated transcriptional feedback repression. Indeed, it is plausible that an important role of CRY may be to suppress daily changes in cytosolic macromolecular content and thus maintain osmotic balance more efficiently over the circadian cycle. This would effectively increase the capacity of WT cells to respond appropriately to any acute stimulus that requires change in proteome composition e.g. insulin/IGF-1 signalling [8].

CRY-deficient cells are more sensitive to proteotoxic stress

The viability of CKO cells and mice clearly suggests that they do maintain protein homeostasis overall, despite proteome imbalance and an altered set point for protein homeostasis compared with WT controls. Proteome imbalance typically renders cells more sensitive to stress [3]. Using ranked GO analysis of overall protein fold-changes compared with WT, we found that the expression of proteins involved in “response to stress” was increased in CKO cells (Figure S6A), suggesting that the proteostasis network in CKO cells is in an activated state [66,72,73].

We therefore hypothesised that CKO cells may be more susceptible to proteotoxic stress. To test this, we probed WT and CKO cells for phosphorylation of eIF2α, a well-characterised marker of the integrated stress response (ISR). As a control we treated cells with tunicamycin, which gradually induces the integrated stress response *via* inhibition of secretory pathway protein glycosylation [74,75]. We observed increased eIF2α phosphorylation in CKO compared with WT cells, at all timepoints (Figure 5A-B). This is strongly indicative of increased proteotoxic stress in these CKO cells.

We note that in most cases eIF2α phosphorylation is known to acutely suppress translation [72], yet we observed a net increase of protein synthesis in CKO cells (Figure 3C, S4D-E). This may be reconciled by our observation that density regulated protein (DENR) and eIF2A, additional alternative subunits of the translation initiation complex, were significantly upregulated in CKO cells compared with WT (Figure S6B-C); and suggests a mechanism whereby chronically stressed CKO cells may overcome increased basal eIF2α phosphorylation, that normally only occurs under acute stress [76–79].

We next sought to test whether increased stress was associated with CRY-deficiency in mouse tissues. STAT3 is a transcription factor that whose phosphorylation on Tyr705 is a well-established inflammatory marker for both chronic and acute cellular stress *in vivo,* across a range of cell types [80–82]. We therefore probed for phosphorylated STAT3 in mouse lungs 5 hours after intraperitoneal injection of bortezomib (BTZ, proteasome inhibitor) or vehicle (control). Compared with WT tissue, we observed increased STAT3 phosphorylation in control CKO mouse lungs, which was further elevated above WT upon BTZ treatment (Figure 5C-D). This shows CRY-deficiency is associated with increased stress and increased sensitivity to stress in mouse tissue, as well as cultured primary cells.

Proteotoxic stress impairs rhythmic robustness

Daily rhythms of PER2 activity in CKO cells (as measured by PER2::LUC bioluminescence) are less robust than in WT cells, being more variable in their expression and damping more rapidly [33]. At the outset of this investigation, we asked how CRY confers increased robustness upon cellular circadian rhythms observed in WT cells, and found evidence suggesting that proteome imbalance in CRY-deficient cells renders them more sensitive to stress. Noting that several different cellular stressors (reductive, oxidative, metabolic, transcriptional inhibition) have previously been reported to reversibly attenuate the expression of cellular circadian rhythms [83,84], our observations suggested the hypothesis that the altered set point of protein homeostasis in CKO renders them more susceptible to stress, which in turn leads to their reduced rhythmic robustness. This informed the prediction that circadian rhythms in WT cells would be less robust, and therefore damp more rapidly, when subject to chronic proteotoxic stress. To test this we monitored PER2::LUC rhythms in WT cells where proteotoxic stress was elicited by sustained inhibition of three different pathways: with epoxomicin (proteasome inhibitor), tunicamycin (unfolded protein ER stress response) or radicicol (HSP90 inhibitor). Consistent with our hypothesis, we observed significantly increased damping rate in treated cells compared with controls, which was reversible upon drug removal by a media change (Figure 6A-F). Thus, chronic proteotoxic stress is sufficient to impair robustness of circadian rhythms, and in principle this may contribute to the reduced robustness and timekeeping fidelity of CKO cells and tissues, as well as diverse CKO mouse phenotypes (Figure 6G, S6D-G, S7).

Discussion

CRY defends cellular homeostasis, which is permissive for robust circadian rhythms

In order to understand the reduced robustness of circadian rhythms in CRY-deficient cells we used several complementary mass spectrometry techniques. We found the abundance of most cellular proteins and protein phosphorylation, as well as the major cellular osmolyte (K^+), to be profoundly perturbed by CRY-deficiency. This was associated with adaptations such as reduced proteasome activity and phosphatase abundance that alter the relative rates of protein synthesis/degradation, and phosphorylation/dephosphorylation, respectively. This results in altered osmotic homeostasis and a state of proteome imbalance compared with WT cells. Proteome imbalance is established as predisposing cells to stress [54,85,86] and is therefore very likely responsible for the increased proteotoxic stress and sensitivity to stress observed in CKO cells. Increased proteotoxic stress by three different mechanisms was sufficient to impair robustness of WT cellular circadian rhythms. Our data therefore suggest that proteome imbalance and associated stress are most likely responsible for the impaired timekeeping fidelity and reduced robustness of CKO cells and tissues *ex vivo.*

CRY proteins are well-characterised as rather promiscuous transcriptional repressors [42,45,87] as well as being selective E3 ubiquitin ligase adaptors [24,88]. Considering the diverse phenotypes, pathologies and proteome changes reported for other E3 ligase adaptor and transcriptional repressor knockout mice [89–93], it is not surprising that the deletion of both *Cryptochrome* genes results in a similarly diverse range of phenotypes; especially when considering the very many identified targets and interacting proteins of CRY1 and CRY2 [24,42,45,87,88].

Proteome imbalance is already very strongly, and in some cases causally, linked to a range of pathological conditions including chronic inflammation, various cancers, metabolic disorders and neurodegeneration [4,54,94–99]. It is therefore quite plausible that proteome imbalance underlies the diverse range of phenotypes exhibited by CKO mice, including impaired body growth [100,101],

increased susceptibility to multiple cancers [102–105], chronic inflammation [106–108] and dysregulated insulin secretion/fat deposition on high fat diets [109]. Indeed, during the course of this research we observed that not only do CKO mice eat more and gain less weight than their isogenic WT counterparts, but they also succumbed to spontaneous mortality/morbidity with a much higher frequency (Figure S6D-G).

CRY suppresses circadian rhythms in protein abundance and osmotic balance

We also noticed that the profound alteration of cellular (phospho)proteome and ionic composition of CKO cells included a complete reorganisation of the subset of proteins and phosphoproteins that are subject to circadian regulation. To our surprise, roughly twice as many proteins and phosphopeptides were rhythmic in CKO cells compared with WT, but only a small minority of rhythmic species were common to both genotypes. We also found that significant changes in the overall abundance of a given protein or phosphopeptide were associated with a change in rhythmicity. The parsimonious interpretation of our findings is that, directly or indirectly, CRY normally functions to suppress rhythms in the abundance of a substantial proportion (19%) of detected cellular proteins, possibly by coupling rhythms of their synthesis and degradation to maintain a dynamic steady state with rhythmic flux (Figure S2A). Removing CRY unmasks the circadian rhythm for these proteins, with most (>80%) changing in overall abundance, due to the new steady state equilibrium that results from a change in the average rate of protein synthesis relative to degradation.

Importantly, we did observe a smaller proportion of cellular proteins (6% total), upon which CRY normally confers rhythmic abundance and which lose that rhythm when CRY is absent; consistent with the more canonical view of CRY function within the TTFL model for circadian rhythms. The majority of these proteins detected (>80% of 6%) also changed in overall abundance when CRY is absent, achieving a new equilibrium concentration for the same reason as those proteins where rhythmic abundance is suppressed by CRY (Figure S2A).

The hypothesis that CRY proteins primarily function to suppress, not generate, variation in protein abundance is further supported by *post-hoc* analysis of published data from mouse liver collected under diurnal cycles and quantified by an independent method [12]. If this hypothesis is correct, it informs the explicit prediction that, in wild type cells, a much greater proportion of proteins are subject to phase-coherent circadian regulation of synthesis/degradation than is apparent from their steady state abundance (Figure S7B). The same logic applies for protein (de)phosphorylation, and these predictions will be a major focus of our future investigations.

We also found that, compared to WT, CKO cells have increased protein abundance and reduced K^+ levels overall, as well as higher amplitude rhythms of cytosolic protein and K^+. Changes in soluble protein concentration require stoichiometrically larger changes in ion concentration to maintain osmotic homeostasis [69]. We therefore suggest that CKO cells may have an impaired ability to buffer changes in intracellular osmolarity, particularly in response to external stimuli, which may contribute to their increased sensitivity to stress [110,111] and attenuated but prolonged response to growth factor stimulation [8]. Overall, our findings have significant implications for the role of CRY proteins specifically, and the canonical TTFL more generally, as well as opening several important avenues for future investigation.

The utility of circadian rhythms for cellular proteostasis

It is frequently suggested that the adaptive advantage of cellular circadian clocks is to anticipate the differential demands of day and night, by turning on genes to accommodate the anticipated increase in demand for the activity of the encoded protein [112]. Protein synthesis is the most energetically expensive process that most cells undertake however, and multiple mechanisms exist to inactivate and sequester proteins that are not required [1,86]. Moreover, recent reports favour the view that changes in cellular transcriptomes function to buffer cellular proteomes, not perturb them [19,20,113]. Rather than

401 synthesise proteins as and when needed, it makes evolutionary sense that cells would expend energy
402 to ensure a constant abundance of most proteins, which could then be mobilised on demand.
403
404 However costly though, damaged/misfolded proteins and activated signal transducers do need to be
405 degraded and replaced to avoid deleterious consequences, such as aggregation and sustained pathway
406 activation. We therefore hypothesise that, rather than rhythm generation, a fundamental advantage
407 conferred on mammalian cells by the daily regulation of CRY activity, within and beyond the
408 canonical TTFL circuit, is the temporal consolidation of proteome renewal, matching synthesis and
409 degradation rates to keep protein concentrations constant and maintain protein homeostasis overall.
410 Indeed, synchronised daily increases in protein synthesis and degradation are likely to be a
411 prerequisite for the efficient assembly of macromolecular protein complexes [114]. Supporting this
412 hypothesis, temporal consolidation of proteome renewal has been observed in yeast cells during their
413 metabolic cycle, a biological oscillation that shares many key features with circadian rhythms in
414 mammalian and other eukaryotic cells [67]. This hypothesis leads to the direct prediction that
415 macromolecular complex assembly will be less efficient and more energetically expensive in cells
416 and tissues that lack the capacity for daily regulation of gene expression cycles, such as Cry1/2, Per1/2
417 and Bmal1-knockouts.
418
419 **Caveats to our findings**
420 In this investigation, we specifically addressed how the steady state circadian cellular
421 (phospho)proteome adapts to CRY deficiency in order to understand the impairment to cellular
422 timekeeping. For this reason, we did not investigate transcriptional regulation in CKO cells, which
423 we believe has been adequately characterised in excellent previous work [25,26,28,33,115–118]. Moreover
424 the generally poor correlation between changes in transcript abundance with protein activity [19,119–122]
425 means that causal relationships cannot be reliably inferred in any case. Thus, we do not exclude that
426 circadian regulation of transcription occurs in CRY-deficient cells, indeed we have observed rhythms

in the activity of the *Nr1d1* promoter in CKO cells, albeit under very specific culture conditions with <5% the amplitude of WT controls [33]. Rather, the increased number and amplitude of protein abundances and phosphorylation we observed in CRY-deficient cells simply cannot be attributed to canonical CRY/PER-mediated transcriptional feedback repression, since CRY is not present and PER does not repress BMAL1 complexes without CRY [22,23]. We also have not addressed the nature of the post-translational mechanism postulated to generate circadian rhythms in mammalian cells, which is discussed elsewhere [7,33].

A further caveat to our study is that, for technical reasons, the primary fibroblasts used for (phospho)proteomics came from a single, but otherwise isogenic, WT and CKO mouse. In our previous work, we have demonstrated circadian rhythms in many independently generated CKO fibroblast lines and tissues, isolated from many different mice [33]. Furthermore, analysis of published mouse liver data provides an independent validation of our finding that CRY primarily functions to supress, not generate, daily protein variation. Moreover, the null hypothesis for this aspect of our analysis was either no rhythms or severely attenuated rhythms in CKO cells, as opposed to higher amplitude rhythms in more proteins, which was subsequently validated by independent methods in separate experiments (cytosolic [protein], & $[K^+]$). Therefore, the most parsimonious interpretation of our findings is that CRY functions primarily to oppose daily protein abundance rhythms, rather than generate them, and thereby buffer cellular protein homeostasis over each daily cycle. We are not aware of any evidence to contradict this interpretation and have no reason to believe that there was anything special about the particular primary CKO fibroblasts used in this study.

It is quite plausible, however, that the numbers and specific identity of many rhythmic (phospho)proteins would vary between independently isolated lines due to stochastic heterogeneity and clonal expansion effects, as also occurs with wild type cells [123,124]. It is also true that the numbers, identities and amplitudes of rhythmic proteins will inevitably vary somewhat, dependent on the

method of analysis used to determine rhythmicity (Figure S1B). It is not plausible, however, that a different method of rhythmicity analysis would yield a qualitatively different result. Moreover, our findings have a clear precedent in that oscillations of protein synthesis and degradation stimulate facilitatory metabolism and compensatory ion transport to maintain osmotic and protein homeostasis during the metabolic cycle of yeast cells [67]. Indeed, the many mechanistic features shared between mammalian circadian rhythms and yeast respiratory oscillations may indicate a common ancestral origin [125].

In our kinase inference analysis, we were surprised not to find evidence supportive of circadian phosphorylation by casein kinase 1 or any of the other kinases implicated in the post-translational circadian regulation. Indeed, the very poor overlap in rhythmically phosphorylated proteins between the two genotypes, and between rhythmic phosphorylation and rhythmic protein in either genotype, suggests that the circadian functions of this post-translational modification are likely to be context-dependent. As with the proteome, however, we did notice a highly significant association between change in rhythmicity and change in phosphopeptide abundance. If a similar interpretation to that which we propose for the proteome were true, it would imply that as much as 20% of protein phosphorylation is subject to cell-autonomous circadian regulation (Figure S2D), and in most cases it is matched by a dephosphorylation rhythm of similar phase and amplitude. Given the consolidation of phosphorylation rhythms around a temporal window that anticipates the active phase (Figure 2G), we speculate that the co-ordinated phase-coherent circadian regulation of phosphorylation and dephosphorylation at many phosphosites, without change in their steady state phosphorylation level, might confer more sensitive and rapid transduction of a given extracellular stimulus when received around the rest-to-active transition compared with 12 hours later. Future work will be required to test this hypothesis experimentally.

Conclusion

In conclusion, we have shown that CRY-dependent feedback mechanisms are not required for cell-autonomous circadian rhythms of protein abundance or phosphorylation in mammalian cells. Moreover, when CRY is present, it functions to suppress more abundance rhythms than it facilitates both *ex vivo* and *in vivo*. CRY-deficiency was associated with an overall imbalance of the proteome, through changes in protein stoichiometries, reduced proteasome activity, increased protein synthesis and overall protein levels. Cells adapt to this genetic insult by altering osmotic balance and proteome composition to achieve a different set point for protein homeostasis, with increased basal stress and sensitivity to proteotoxic stress. This likely accounts for the impairment of circadian timekeeping in CKO cells, tissues and mice, and may also contribute to the (patho)physiological consequences of CRY-deficiency in mice. We speculate that the principal utility of CRY-mediated feedback repression is to couple global protein synthesis with degradation rates for most proteins, to minimise changes in protein abundance. This would ensure the energetically efficient temporal consolidation of proteome renewal during each day, whilst defending protein and osmotic homeostasis.

Methods

Mammalian cell culture

All animal work was licensed by the Home Office under the Animals (Scientific Procedures) Act 1986, with Local Ethical Review by the Medical Research Council and the University of Cambridge, UK. Fibroblasts homozygous for PER2::LUCIFERASE [126] were extracted from adult mouse lung tissue and then serial passage was used as described previously to induce spontaneous immortalisation [125,127]. Fibroblasts were cultured in Dulbecco's Modified Eagle Medium (DMEM), supplemented with 100 units/ml penicillin, 100 µg/ml streptomycin (Gibco) and 10% FetalClone III serum (HyClone, Thermo Fisher). All cells were confirmed to be free of Mycoplasma. Unless stated otherwise, confluent cell cultures up to a maximum of 30 passages were used during experiments to abolish any effects of cell division, since these cells display contact inhibition.

General statistics

P values are annotated in figures with asterisks, where the number of asterisks indicates the significance: Ns = not significant; * = $p \leq 0.05$; ** = $p \leq 0.01$, *** = $p \leq 0.001$; **** = $p \leq 0.0001$. Technical replicates are denoted as "n" in the figures or figure legends (e.g. n=3), and biological replicates are denoted as "N". Statistical tests were carried out using Prism Graphpad 8 (San Diego, Ca) or R v4.0.3.

Longitudinal bioluminescent reporter experiments

Data from longitudinal bioluminescence recordings were analysed using Prism Graphpad 8 (San Diego, Ca). A 24-hour moving average was used to detrend data, and a circadian damped cosine wave was fitted by least-squares regression to determine period, phase and amplitude:

$$y = (mx + c) + a\, e^{-kx} \cos\left(\frac{2\pi x - r}{p}\right)$$

Where *m* is the baseline gradient, *c* is the displacement in the *y* axis, *k* is the damping rate, *a* is the amplitude, *r* is the phase and *p* is the period. The first 24 hours of each recording were omitted because this represents the transient effects of medium change on clock gene expression. Rhythmicity of bioluminescence recordings was assessed by comparing the fit of this equation to the null hypothesis of a straight line using the Extra sum-of-squares F test in Prism Graphpad 8 (San Diego, CA). If fitting to the damped cosine was preferred ($p \leq 0.05$) then the recording was deemed "rhythmic".

Timecourse experiments: general structure

Cells were plated at a near-confluent density (roughly 27,000 cells per cm^2) and cultured in DMEM with 10% FetalClone III serum for one week in a temperature-controlled incubator that was programmed to oscillate between 32°C and 37°C, with transitions every 12 hours. The cells received a medium change at the transition between 37°C and 32°C after 4 days. After another 3 days the cells received another medium change at the same transition time into medium containing either 10% or 1% serum, and the incubator was programmed to remain at 37°C constantly. At this time, a subset of cells received medium containing 1 mM luciferin, and these were placed into an ALLIGATOR for bioluminescent recording. After 24 hours, sampling began, with 3 hour intervals, and continuing for 3 days. The time point of the first sample is known as "Experimental time 0", and all time points are reported relative to this. The nature of the sampling varied according to the specific experiment, and details are presented in separate sections.

Proteomics and phosphoproteomics

Sample preparation

A timecourse was carried out as described above. At each timepoint cells were washed twice in ice cold PBS and then lysed at room temperature in 100 µL lysis buffer (8 M urea, 20 mM Tris, pH 8) for 20 minutes. The lysis buffer was prepared the day before sampling began, and frozen in 1 mL aliquots. At each timepoint, one aliquot was defrosted at room temperature (23°C) whilst shaking at

700 rpm for 5 minutes. After lysis the cells were scraped and technical replicates were combined before flash freezing in liquid nitrogen and storage at -80°C. After defrosting, the samples were sonicated for 2 minutes and the protein concentration was measured using a BCA assay (Pierce). 12 pooled samples were created by combining a portion of each experimental sample such that each sample/pool contained an equal amount of protein. All samples were then flash frozen in liquid nitrogen and stored at -80ºC.

Enzymatic Digestion

Each sample (256 µg) was reduced with 5 mM DTT at 56°C for 30 minutes and then alkylated with 10 mM iodoacetamide in the dark at room temperature for 30 minutes. They were then digested with mass spectrometry grade Lys-C (Promega) at a protein:Lys-C ratio of 100:1 (w/w) for 4 hours at 25°C. Next, the samples were diluted to 1.5 M urea using 20 mM HEPES (pH 8.5) and digested at 30°C overnight with trypsin (Promega) at a ratio of 70:1 (w/w). Digestion was quenched by the addition of trifluoroacetic acid (TFA) to a final concentration of 1%. Any precipitates were removed by centrifugation at 13000g for 15 minutes. The supernatants were desalted using homemade C18 stage tips containing 3M Empore extraction disks (Sigma) and 5 mg of Poros R3 resin (Applied Biosystems). Bound peptides were eluted with 30-80% acetonitrile (MeCN) in 0.1% TFA and lyophilized.

TMT (Tandem mass tag) peptide labelling

The lyophilized peptides from each sample were resuspended in 100 µl of 2.5% MeCN, 250 mM triethylammonium bicarbonate. According to manufacturer's instructions, 0.8 mg of each TMT 10plex reagent (Thermo) was reconstituted in 41 µl of anhydrous MeCN. The peptides from each time point and pooled sample were labelled with a distinct TMT tag for 75 minutes at room temperature. The labelling reaction was quenched by incubation with 8 µl 5% hydroxylamine for 30 min. For each set of 10-plex TMT reagent, the labelled peptides from 8 time point samples + 2 pools

were combined into a single sample and partially dried to remove MeCN in a SpeedVac (Thermo Scientific). After this, the sample was desalted as before and the eluted peptides were lyophilized.

Basic pH Reverse-Phase HPLC fractionation

The TMT labelled peptides were subjected to off-line High Performance Liquid Chromatography (HPLC) fractionation, using an XBridge BEH130 C18, 3.5 µm, 4.6 mm x 250 mm column with an XBridge BEH C18 3.5 µm Van Guard cartridge (Waters), connected to an Ultimate 3000 Nano/Capillary LC System (Dionex). Peptide mixtures were resolubilized in solvent A (5% MeCN, 95% 10 mM ammonium bicarbonate, pH 8) and separated with a gradient of 1-90% solvent B (90% MeCN, 10% 10 mM ammonium bicarbonate, pH 8) over 60 minutes at a flow rate of 500 µl/min. A total of 60 fractions were collected. They were combined into 20 fractions and lyophilized and desalted as before. 5% of the total eluate from each fraction was taken out for proteome LC-MS/MS analysis and the rest was used for phosphopeptide enrichment.

Enrichment of phosphopeptides

All 20 fractions of peptide mixture were enriched first using PHOS-Select iron affinity gel, an Iron (III) Immobilised Metal Chelate Affinity Chromatography (IMAC) resin (Sigma). Desalted peptides were resuspended in 30% MeCN, 0.25 M acetic acid (loading solution) and 30 µl of IMAC beads, previously equilibrated with the loading solution, was added. After 60 minutes incubation at room temperature, beads were transferred to a homemade C8 (3M Empore) stage tip and washed 3 times with loading solution. Phosphopeptides were eluted sequentially with 0.4 M NH_3, 30% MeCN, 0.4 M NH_3 and 20 µl of 50% MeCN, 0.1% TFA.

The flow-through from the C8 stage tips was collected and combined into 10 fractions and used for titanium dioxide (TiO_2) phosphopeptide enrichment. For this, the total volume of flow-through was made up to 50% MeCN, 2 M lactic acid (loading buffer) and incubated with 1-2 mg TiO_2 beads

(Titansphere, GL Sciences, Japan) at room temperature for 1 hour. The beads were transferred into C8 stage tips, washed in the tip twice with the loading buffer and once with 50% MeCN, 0.1% TFA. Phosphopeptides were then eluted sequentially with 50 mM K_2HPO_4 (pH 10) followed by 50% MeCN, 50 mM K_2HPO_4 (pH 10) and 50% MeCN, 0.1% TFA.

The first 10 fractions of IMAC and the 10 fractions of TiO_2 enriched phosphopeptides were combined, and the other 10 fractions from IMAC enrichment were combined into 5 fractions, thus making a total of 15 fractions for phosphoproteomics analysis. Phosphopeptide solution from these fractions were acidified, partially dried, and desalted with a C18 Stage tip that contained 1.5 µl of Poros R3 resin. These were then partially dried again and thus ready for mass spectrometry analysis.

LC MS/MS

The fractionated peptides were analysed by LC-MS/MS using a fully automated Ultimate 3000 RSLC nano System (Thermo) fitted with a 100 µm x 2 cm PepMap100 C18 nano trap column and a 75 µm × 25 cm reverse phase C18 nano column (Aclaim PepMap, Thermo). Samples were separated using a binary gradient consisting of buffer A (2% MeCN, 0.1% formic acid) and buffer B (80% MeCN, 0.1% formic acid), and eluted at 300 nL/min with an acetonitrile gradient. The outlet of the nano column was directly interfaced via a nanospray ion source to a Q Exactive Plus mass spectrometer (Thermo). The mass spectrometer was operated in standard data-dependent mode, performing a MS full-scan in the m/z range of 350-1600, with a resolution of 70000. This was followed by MS2 acquisitions of the 15 most intense ions with a resolution of 35000 and Normalised Collision Energy (NCE) of 33%. MS target values of 3e6 and MS2 target values of 1e5 were used. The isolation window of precursor ion was set at 0.7 Da and sequenced peptides were excluded for 40 seconds.

622 ***Spectral processing and peptide and protein identification***

623 The acquired raw files from LC-MS/MS were processed using MaxQuant (Cox and Mann) with the
624 integrated Andromeda search engine (v1.6.3.3). MS/MS spectra were quantified with reporter ion
625 MS2 from TMT 10plex experiments and searched against the *Mus musculus* UniProt Fasta database
626 (Dec 2016). Carbamidomethylation of cysteines was set as fixed modification, while methionine
627 oxidation, N-terminal acetylation and phosphorylation (STY) (for phosphoproteomics group only)
628 were set as variable modifications. Protein quantification requirements were set at 1 unique and razor
629 peptide. In the identification tab, second peptides and match between runs were not selected. Other
630 parameters in MaxQuant were set to default values.
631
632 The MaxQuant output file was then processed with Perseus (v1.6.2.3). Reporter ion intensities were
633 uploaded to Perseus. The data was filtered: identifications from the reverse database were removed,
634 only identified by site, potential contaminants were removed, and we only considered proteins with
635 ≥1 unique and razor peptide. Then all columns with an intensity "less or equal to zero" were converted
636 to "NAN" and exported. The MaxQuant output file with phosphor (STY) sites table was also
637 processed with Perseus software (v1.6.2.3). The data was filtered: identifications from the reverse
638 database were removed, only identified by site, potential contaminants were removed and we only
639 considered phosphopeptides with localization probability ≥ 0.75. Then all columns with intensity
640 "less or equal to zero" were converted to "NAN" and exported.
641
642 ***Bioinformatics***

643 All data handling was done using R v3.6.3. Since the sample for timepoint 12 was missing for CRY1$^{-/-}$;
644 CRY2$^{-/-}$, abundance values were inferred for each protein by taking the mean of the two
645 neighbouring timepoints. WT and CKO datasets were analysed either combined or independently.
646 The combined analysis was used to directly compare protein and phosphopeptide abundances
647 between genotypes, since the internal reference scaling normalisation accounts for batch effects. The

independent method was used for all other analysis that did not require comparison of abundance, thus allowing the detection of proteins that were present in one genotype but not the other.

Proteins and phosphopeptides were only accepted for further analysis if present in all timepoints and pooled samples. Hence in the combined analysis, proteins/phosphopeptides had to be present in all timepoints for both genotypes, as well as all pooled samples. In the independent analysis, proteins/phosphopeptides had to be present in all timepoints and pools for one genotype only. Sample loading normalisation was carried out by taking the sum of all intensities for each time point and normalising to the mean of these, since an equal amount of protein was used for each TMT labelling reaction. This was followed by internal reference scaling (IRS) to allow for comparisons between TMT experiments [128]: for each TMT 10plex set the mean abundance for each protein in both pools was calculated. Then the mean of these means was calculated and used to normalise the values for each protein for all the samples.

Rhythmicity was tested using the RAIN (Rhythmicity Analysis Incorporating Non-parametric methods) algorithm [129], and multiple testing was corrected for using the adaptive Benjamini-Hochberg method. Proteins with a corrected $p \leq 0.05$ were deemed significant. Relative amplitude of rhythmic proteins was calculated by detrending the data using a 24-hour moving average and dividing the resultant range by the average normalised protein abundance. To include only proteins with a biologically relevant level of oscillation, only those with relative amplitude $\geq 10\%$ were taken for further analysis (see text for details). Phosphoproteomics data were handled in the same way, except that normalised phosphopeptide abundances were adjusted according to the changes in abundance of the corresponding protein from the normalised total proteome data, and no threshold for relative amplitude was used.

673 Gene ontology analysis was performed using the GOrilla online tool [130,131]. Analysis was performed
674 either as a single ranked list of gene names, or as a target dataset compared to background (all proteins
675 detected in the experiment). Kinase recognition motifs were screened using a custom script written
676 in Python v2.7, which used the PHOSIDA database [52,53]. Scripts and processed data are available on
677 GitHub (https://github.com/davwong47/Circadian-proteomics). Mass spectrometry data have been
678 deposited to the ProteomeXchange Consortium [132] via the PRIDE [133] partner repository with the
679 dataset identifier PXD019499.
680
681 **Western blotting**
682 For Western blots, proteins were run on NuPAGE™ Novex™ 4-12% Bis-Tris Protein Gels (Thermo
683 Fisher) before transferring to nitrocellulose membranes. For transfer, the iBlot system (Thermo Fisher)
684 was used. Membranes were blocked using 5% milk powder (Marvel) or 0.125% BSA (Sigma) and
685 0.125% milk powder (Marvel) in TBS containing 0.1% Tween-20 (TBST) for 30 minutes at room
686 temperature then incubated with primary antibody at 4°C overnight. HRP-conjugated secondary
687 antibodies (Thermo Fisher) diluted 1:10000 in blocking buffer were incubated with the blots for 1
688 hour at room temperature. Chemiluminescence was detected in a Biorad chemidoc using Immobilon
689 reagent (Millipore). Protein loading was checked by staining gels with Colloidal Coomassie Blue
690 Stain (Severn Biotech). Densitometric analysis was carried out using Image Lab 4.1 (Biorad
691 Laboratories 2012).
692
693 **Measurement of cellular protein content**
694 At specified time points, confluent monolayers of cells were washed twice with ice-cold PBS. Cells
695 were then incubated with 200 µL digitonin lysis buffer (50 mM Tris pH 7.4, 0.01% digitonin, 5 mM
696 EDTA, 150 mM NaCl, 1 U/mL Benzonase, protease and phosphatase inhibitors) on ice for 15 minutes
697 before lysates were collected. For total protein extraction, cells were instead incubated with 200 µL
698 RIPA buffer (50 mM Tris pH 7.4, 1% SDS, 5 mM EDTA, 150 mM NaCl, 1 U/mL Benzonase,

699 protease and phosphatase inhibitors), on ice for 15 minutes. Cells lysed with RIPA buffer were then
700 scraped and collected and all samples were flash frozen in liquid nitrogen. After thawing, RIPA
701 lysates were sonicated at high power for 10 seconds at 4°C to shear genomic DNA. RIPA lysates and
702 digitonin lysates were clarified by centrifugation at 21,000 g for 15 minutes at 4°C.
703
704 Intrinsic tryptophan fluorescence was used to measure protein concentrations. 10 µL of each sample
705 was transferred into a UV-transparent 384 well plate (Corning 4681) in quadruplicate. After brief
706 centrifugation of the plate, quantification was carried out using a Tecan Spark 10M microplate reader,
707 with excitation at 280 nm and emission at 350 nm. Standards were made using bovine serum albumin
708 (Fisher Scientific), dissolved using the same lysis buffer as the lysates being measured. Standard
709 curves were fitted to a quadratic curve using Prism Graphpad 8 (San Diego, Ca), and protein
710 concentrations were interpolated.
711
712 **Measurement of intracellular ion content by Inductively Coupled Plasma - Mass Spectrometry**
713 **(ICP-MS)**
714 Confluent monolayers of cells were washed on ice with iso-osmotic buffer A (300 mM sucrose, 10
715 mM Tris base, 1 mM EDTA, pH 7.4 adjusted with phosphoric acid, 330-340 mOsm adjusted with
716 sucrose/HPLC water), followed by iso-osmotic buffer B (300 mM sucrose, 10 mM Tris base, 1 mM
717 EDTA, pH 7.4 adjusted with acetic acid, 330-340 mOsm adjusted with sucrose/HPLC water). Iso-
718 osmotic buffer A contains phosphoric acid which displaces lipid bound ions. Iso-osmotic buffer B
719 contains acetic acid which removes traces of phosphates. Cells were then incubated for 30 minutes at
720 room temperature in 200 µL ICP-MS cell lysis buffer (65% nitric acid, 0.1 mg/mL (100 ppb) cerium).
721 Lysates were then collected and stored at -80°C. All samples were thawed simultaneously and diluted
722 using HPLC water to a final concentration of 5% nitric acid. Diluted samples were analysed by
723 Inductively Coupled Plasma - Mass Spectrometry (ICP-MS) using the NexION 350D ICP-MS
724 (PerkinElmer Inc.) as described previously [134].

725

726 **Proteasome activity assays**

727 20,000 cells per well were plated in a 96-well plate using standard culture medium, and on the
728 following day the medium was changed. 10 µM epoxomicin in the medium was used as negative
729 control. 3 hours later, the ProteasomeGlo Cell-Based Assay (Promega) was used to measure
730 proteasome catalytic activity. Chymotrypsin-like, trypsin-like and caspase-like activities were
731 measured separately using the relevant substrates from Promega (Suc-LLVY-Glo, Z-LRR-Glo, Z-
732 nLPnLD-Glo respectively). Assay reagents were prepared according to the manufacturer's
733 instructions. The 96-well plate was equilibrated to room temperature, and a volume of assay reagent
734 equal to the volume of medium was added to each well before shaking at 700 rpm for 2 minutes. The
735 plate was incubated at room temperature for a further 10 minutes, and then luminescence was
736 measured using the Tecan Spark 10M microplate reader, recording counts for 1 second. The
737 luminescence readings from the epoxomicin controls represent background protease activity, and so
738 this was subtracted from all other recordings.

739

740 **Measurement of translation rate**

741 WT and CKO mouse lung fibroblasts were grown to confluence in 48-well plates, and medium was
742 changed 24h before the experiment to either low (1%) or high (10%) serum. The cells were pulsed
743 with 0.1 mCi/ml ^{35}S-L-methionine/^{35}S-L-cysteine mix (EasyTag™ EXPRESS35S Protein Labeling
744 Mix, Perkin Elmer) in cysteine/methionine-free DMEM for 15 min at 37°C, with or without serum
745 supplement. Afterwards, cells were washed with ice-cold PBS and lysed in digitonin-based buffer
746 (with protease inhibitor tablet, added freshly) on ice. Lysates were reduced with LDS buffer and run
747 on 4-12% Bis-Tris SDS-PAGE using MES buffer. Gels were then dried at 80°C and exposed
748 overnight to a phosphorimager screen. Images were acquired with Typhoon FLA700 gel scanner and
749 quantified using Fiji.

750

For the puromycin pulse experiment, cells were seeded (in the presence of 1 mM luciferin) in fibronectin-coated dishes at high density one day before starting the experiment. Separate 6-well plates were used for each time point. 30 minutes before the start of the experiment, cells were synchronised by a dexamethasone pulse (10 nM), after which cells were exchanged into Air medium (DMEM without glucose, L-glutamine, phenol red, sodium pyruvate and sodium bicarbonate (Sigma). The following were added: 0.35 g/L sodium bicarbonate (Sigma), 5 g/L glucose (Sigma), 20 mM MOPS (VWR), penicillin/streptomycin solution (as above), Glutamax (Thermo Fisher), B27 (Thermo Fisher), 1 mM potassium luciferin solution (Biosyth), 1% FetalClone III serum. The medium was adjusted to pH 7.6 at room temperature, and osmolality adjusted to 350-360 mOsm/kg using sodium chloride). At the indicated time points, 10 µg/mL puromycin was added while keeping cells warm on a hot plate, after which the plate was incubated in tissue culture incubator for exactly 10 minutes. Timepoint 0 represents cells just before the dexamethasone pulse. Cells were then washed with ice-cold PBS, after which they were lysed in lysis buffer (50 mM tris, pH 7.5, 1% Triton X-100, 0.1% SDS, 1.5 mM $MgCl_2$, 100 mM NaCl, cOmplete protease inhibitor cocktail (Roche)) and flash frozen. For Western blot analysis, samples were spun down, diluted in Laemmli sample buffer, ran on 4-20% gradient gels, and blots were probed for ATF4 and tubulin.

Animal work

All animals were maintained in 12:12 hour light:dark conditions. Post-mortem histopathology examinations were carried out by Abbey Veterinary Services, UK. For the *in vivo* stress marker experiment, animals received an IP injection of bortezomib (Generon) (2.5 mg/kg) or vehicle control (1% DMSO in sterile PBS) 2 hours after the transition to the light phase. 5 hours later, the animals were culled and lungs were immediately flash frozen in liquid nitrogen. Tissues were homogenised on ice in RIPA buffer (as above) and flash frozen. After thawing these samples on ice, they were sonicated briefly at 4°C. Samples were clarified by centrifugation and protein diluted to 2 mg/mL. Bolt/NuPage loading buffer with 50 mM TCEP (final concentration) was added and reduced for 10

777 minutes at 70°C. Western blots were then carried out as described above, probing against phospho-
778 STAT3 (Tyr705) or actin. One female mouse and one male mouse of each genotype were used in this
779 experiment.

780

781 **Antibodies**

Antibody	Host	Cat. #	Manufacturer	Dilution
Anti-mouse-HRP	Goat	A4416	Sigma	1:10000
Anti-rabbit-HRP	Goat	A6154	Sigma	1:10000
Anti-rat-HRP	Goat	629520	Thermo	1:10000
Tubulin YL1-2	Rat		in-house	1:100
β-Actin	Mouse	sc-47778	Santa-Cruz Biotechnology	1:1000
Proteasome 20S α1-7	Mouse	ab22674	Abcam	1:2000
EIF2α	Mouse	AhO0802	Thermo	1:1000
P-EIF2α (S51)	Rabbit	ab32157	Abcam	1:1000
P-STAT3 (Tyr705)	Rabbit	D3A7	Cell Signaling	1:1000
Histone H3	Rabbit	ab1791	Abcam	1:10000

782

Acknowledgements

We thank biomedical technical staff at Medical Research Council (MRC) Ares facility and LMB facilities for assistance; G.T. van der Horst and J.S. Takahashi for sharing rodent models; Y-G. Suh, M.H. Hastings and E.S. Maywood for providing reagents and input; M. Hegde, E. Zavodszky, R. Edgar, N. Hoyle, M. Coetzee, J. Chesham, A. Hufnagel, P. Crosby, D.S. Tourigny, J.E. Chambers, H.C. Causton and Tim Stevens for assistance with analysis and experiments as well as valuable discussion. DCSW was supported by the MRC Doctoral Training Programme and the Frank Edward Elmore Fund. AS was supported by the AstraZeneca Blue Skies Initiative. NMR was supported by the Medical Research Council (MR/S022023/1). MP was supported by the Dutch Cancer Foundation (KWF, BUIT-2014-6637) and EMBO (ALTF-654-2014). JON was supported by the Medical Research Council (MC_UP_1201/4) and the Wellcome Trust (093734/Z/10/Z).

Contributions

DCSW, ES and JON designed the study, analysed the data and wrote the manuscript; DCSW, ES, AS, AZ and MP performed cell experiments; SPC and JD performed mass spectrometry analyses; DCSW, NMR, ADB and JON performed mouse studies; MR performed tissue collection and husbandry. All authors commented on the manuscript.

Conflicts of interest

The authors declare that they have no conflict of interest.

References

1. Wolff, S., Weissman, J. S. & Dillin, A. Differential Scales of Protein Quality Control. *Cell* **157**, 52–64 (2014).
2. Juszkiewicz, S. & Hegde, R. S. Quality Control of Orphaned Proteins. *Molecular Cell* vol. 71 443–457 (2018).
3. Harper, J. W. & Bennett, E. J. Proteome complexity and the forces that drive proteome imbalance. *Nature* **537**, 328–338 (2016).
4. Labbadia, J. & Morimoto, R. I. The Biology of Proteostasis in Aging and Disease. *Annu. Rev. Biochem.* **84**, 435–464 (2015).
5. Balchin, D., Hayer-Hartl, M. & Hartl, F. U. In vivo aspects of protein folding and quality control. *Science* **353**, aac4354 (2016).
6. Cederroth, C. R. *et al.* Medicine in the Fourth Dimension. *Cell Metabolism* vol. 30 238–250 (2019).
7. Wong, D. C. & O'Neill, J. S. Non-transcriptional processes in circadian rhythm generation. *Curr. Opin. Physiol.* **5**, 117–132 (2018).
8. Crosby, P. *et al.* Insulin/IGF-1 Drives PERIOD Synthesis to Entrain Circadian Rhythms with Feeding Time. *Cell* **177**, 896-909.e20 (2019).
9. Hoyle, N. P. *et al.* Circadian actin dynamics drive rhythmic fibroblast mobilization during wound healing. *Sci. Transl. Med.* **9**, eaal2774 (2017).
10. Reddy, A. B. *et al.* Circadian Orchestration of the Hepatic Proteome. *Curr. Biol.* **16**, 1107–1115 (2006).
11. Robles, M. S., Cox, J. & Mann, M. In-Vivo Quantitative Proteomics Reveals a Key Contribution of Post-Transcriptional Mechanisms to the Circadian Regulation of Liver Metabolism. *PLoS Genet.* **10**, (2014).
12. Mauvoisin, D. *et al.* Circadian clock-dependent and -independent rhythmic proteomes implement distinct diurnal functions in mouse liver. *Proc. Natl. Acad. Sci. U. S. A.* **111**, 167–

72 (2014).

13. Aragón, J. J. & Sols, A. Regulation of enzyme activity in the cell: effect of enzyme concentration. *FASEB J.* **5**, 2945–2950 (1991).

14. Bulik, S., Holzhütter, H. G. & Berndt, N. The relative importance of kinetic mechanisms and variable enzyme abundances for the regulation of hepatic glucose metabolism - insights from mathematical modeling. *BMC Biol.* **14**, (2016).

15. Rocca, J. D. *et al.* Relationships between protein-encoding gene abundance and corresponding process are commonly assumed yet rarely observed. *ISME Journal* vol. 9 1693–1699 (2015).

16. Nadaraia, S., Yohrling, G. J., Jiang, G. C.-T., Flanagan, J. M. & Vrana, K. E. Enzyme Activity: Control. in *Encyclopedia of Life Sciences* (John Wiley & Sons, Ltd, 2007). doi:10.1002/9780470015902.a0000861.pub2.

17. Ukai, H. & Ueda, H. R. Systems Biology of Mammalian Circadian Clocks. *Annu. Rev. Physiol.* **72**, 579–603 (2010).

18. Takahashi, J. S. Transcriptional architecture of the mammalian circadian clock. *Nat. Rev. Genet.* **18**, 164–179 (2016).

19. Liu, Y., Beyer, A. & Aebersold, R. On the Dependency of Cellular Protein Levels on mRNA Abundance. *Cell* vol. 165 535–550 (2016).

20. Franks, A., Airoldi, E. & Slavov, N. Post-transcriptional regulation across human tissues. *PLoS Comput. Biol.* **13**, (2017).

21. Wang, S. H., Hsiao, C. J., Khan, Z. & Pritchard, J. K. Post-translational buffering leads to convergent protein expression levels between primates. *Genome Biol.* **19**, (2018).

22. Ye, R. *et al.* Dual modes of CLOCK:BMAL1 inhibition mediated by Cryptochrome and Period proteins in the mammalian circadian clock. *Genes Dev.* **28**, 1989–98 (2014).

23. Chiou, Y.-Y. *et al.* Mammalian Period represses and de-represses transcription by displacing CLOCK-BMAL1 from promoters in a Cryptochrome-dependent manner. *Proc. Natl. Acad. Sci. U. S. A.* **113**, E6072–E6079 (2016).

24. Correia, S. P. *et al.* The circadian E3 ligase complex SCFFBXL3+CRY targets TLK2. *Sci. Rep.* **9**, 198 (2019).

25. Kume, K. *et al.* mCRY1 and mCRY2 are essential components of the negative limb of the circadian clock feedback loop. *Cell* **98**, 193–205 (1999).

26. Sato, T. K. *et al.* Feedback repression is required for mammalian circadian clock function. *Nat. Genet.* **38**, 312–319 (2006).

27. van der Horst, G. T. *et al.* Mammalian Cry1 and Cry2 are essential for maintenance of circadian rhythms. *Nature* **398**, 627–30 (1999).

28. Ukai-Tadenuma, M. *et al.* Delay in feedback repression by cryptochrome 1 Is required for circadian clock function. *Cell* **144**, 268–281 (2011).

29. Ode, K. L. *et al.* Knockout-Rescue Embryonic Stem Cell-Derived Mouse Reveals Circadian-Period Control by Quality and Quantity of CRY1. *Mol. Cell* **65**, 176–190 (2017).

30. Cox, K. H. & Takahashi, J. S. Circadian clock genes and the transcriptional architecture of the clock mechanism. *J. Mol. Endocrinol.* **63**, R93–R102 (2019).

31. Maywood, E. S., Chesham, J. E., O'Brien, J. A. & Hastings, M. H. A diversity of paracrine signals sustains molecular circadian cycling in suprachiasmatic nucleus circuits. *Proc. Natl. Acad. Sci.* **108**, 14306–14311 (2011).

32. Ono, D., Honma, S. & Honma, K. Cryptochromes are critical for the development of coherent circadian rhythms in the mouse suprachiasmatic nucleus. *Nat. Commun.* **4**, 1666 (2013).

33. Putker, M. *et al.* CRYPTOCHROMES confer robustness, not rhythmicity, to circadian timekeeping. *EMBO J.* **e106745**, 1–15 (2021).

34. Beale, A. D. *et al.* Casein Kinase 1 Underlies Temperature Compensation of Circadian Rhythms in Human Red Blood Cells. *J. Biol. Rhythms* **34**, 144–153 (2019).

35. Cho, C.-S., Yoon, H. J., Kim, J. Y., Woo, H. A. & Rhee, S. G. Circadian rhythm of hyperoxidized peroxiredoxin II is determined by hemoglobin autoxidation and the 20S proteasome in red blood cells. *Proc. Natl. Acad. Sci.* **111**, 12043–12048 (2014).

882 36. Henslee, E. A. *et al.* Rhythmic potassium transport regulates the circadian clock in human red
883 blood cells. *Nat. Commun.* **8**, 1978 (2017).
884 37. Ray, S. *et al.* Circadian rhythms in the absence of the clock gene Bmal1. *Science (80-.).* **367**,
885 800–806 (2020).
886 38. Lipton, J. O. *et al.* The Circadian Protein BMAL1 Regulates Translation in Response to S6K1-
887 Mediated Phosphorylation. *Cell* **161**, 1138–1151 (2015).
888 39. Yu, E. A. & Weaver, D. R. Disrupting the circadian clock: Gene-specific effects on aging,
889 cancer, and other phenotypes. *Aging* vol. 3 479–493 (2011).
890 40. Maury, E., Ramsey, K. M. & Bass, J. Circadian rhythms and metabolic syndrome: From
891 experimental genetics to human disease. *Circulation Research* vol. 106 447–462 (2010).
892 41. Mauvoisin, D. *et al.* Circadian and Feeding Rhythms Orchestrate the Diurnal Liver Acetylome.
893 *Cell Rep.* **20**, 1729–1743 (2017).
894 42. Kriebs, A. *et al.* Circadian repressors CRY1 and CRY2 broadly interact with nuclear receptors
895 and modulate transcriptional activity. *Proc. Natl. Acad. Sci.* **114**, 8776–8781 (2017).
896 43. Papp, S. J. *et al.* DNA damage shifts circadian clock time via hausp-dependent cry1
897 stabilization. *Elife* **2015**, 1–19 (2015).
898 44. Jordan, S. D. *et al.* CRY1/2 Selectively Repress PPARδ and Limit Exercise Capacity. *Cell*
899 *Metab.* **26**, 243-255.e6 (2017).
900 45. Koike, N. *et al.* Transcriptional architecture and chromatin landscape of the core circadian
901 clock in mammals. *Science* **338**, 349–54 (2012).
902 46. Elowitz, M. B., Levine, A. J., Siggia, E. D. & Swain, P. S. Stochastic gene expression in a
903 single cell. *Science (80-.).* **297**, 1183–1186 (2002).
904 47. Raser, J. M. & O'Shea, E. K. Control of stochasticity in eukaryotic gene expression. *Science*
905 *(80-.).* **304**, 1811–1814 (2004).
906 48. Volfson, D. *et al.* Origins of extrinsic variability in eukaryotic gene expression. *Nature* **439**,
907 861–864 (2006).

908 49. Sigal, A. *et al.* Variability and memory of protein levels in human cells. *Nature* **444**, 643–646
909 (2006).
910 50. Pedraza, J. H. & Van Oudenaarden, A. Noise propagations in gene networks. *Science (80-.).*
911 **307**, 1965–1969 (2005).
912 51. Robles, M. S., Humphrey, S. J. & Mann, M. Phosphorylation Is a Central Mechanism for
913 Circadian Control of Metabolism and Physiology. *Cell Metab.* **0**, 35–48 (2016).
914 52. Gnad, F., Gunawardena, J. & Mann, M. PHOSIDA 2011: The posttranslational modification
915 database. *Nucleic Acids Res.* **39**, 253–260 (2011).
916 53. Gnad, F. *et al.* PHOSIDA (phosphorylation site database): Management, structural and
917 evolutionary investigation, and prediction of phosphosites. *Genome Biol.* **8**, (2007).
918 54. Harper, J. W. & Bennett, E. J. Proteome complexity and the forces that drive proteome
919 imbalance. *Nature* **537**, 328–338 (2016).
920 55. Fortelny, N., Overall, C. M., Pavlidis, P. & Freue, G. V. C. Can we predict protein from mRNA
921 levels? *Nature* **547**, E19–E20 (2017).
922 56. Stitt, M. & Gibon, Y. Why measure enzyme activities in the era of systems biology? *Trends*
923 *in Plant Science* vol. 19 256–265 (2014).
924 57. Brunner, A.-D. *et al.* Ultra-high sensitivity mass spectrometry quantifies single-cell proteome
925 changes upon perturbation. *bioRxiv* 2020.12.22.423933 (2021)
926 doi:10.1101/2020.12.22.423933.
927 58. Deery, M. J. *et al.* Proteomic analysis reveals the role of synaptic vesicle cycling in sustaining
928 the suprachiasmatic circadian clock. *Curr. Biol.* **19**, 2031–6 (2009).
929 59. Rey, G. *et al.* Metabolic oscillations on the circadian time scale in Drosophila cells lacking
930 clock genes. *Mol. Syst. Biol.* **14**, e8376 (2018).
931 60. Hurley, J. M. *et al.* Circadian Proteomic Analysis Uncovers Mechanisms of Post-
932 Transcriptional Regulation in Metabolic Pathways. *Cell Syst.* **7**, 613-626.e5 (2018).
933 61. Vogel, C. & Marcotte, E. M. Insights into the regulation of protein abundance from proteomic

and transcriptomic analyses. *Nat. Rev. Genet.* **13**, 227–232 (2012).

62. Buccitelli, C. & Selbach, M. mRNAs, proteins and the emerging principles of gene expression control. *Nat. Rev. Genet.* **21**, 630–644 (2020).

63. Schwanhäusser, B. *et al.* Global quantification of mammalian gene expression control. *Nature* **473**, 337–342 (2011).

64. Liu, Y., Beyer, A. & Aebersold, R. On the Dependency of Cellular Protein Levels on mRNA Abundance. *Cell* **165**, 535–550 (2016).

65. Morimoto, R. I. & Cuervo, A. M. Protein homeostasis and aging: Taking care of proteins from the cradle to the grave. in *Journals of Gerontology - Series A Biological Sciences and Medical Sciences* vol. 64 167–170 (J Gerontol A Biol Sci Med Sci, 2009).

66. Klaips, C. L., Jayaraj, G. G. & Hartl, F. U. Pathways of cellular proteostasis in aging and disease. *Journal of Cell Biology* vol. 217 51–63 (2018).

67. O'Neill, J. S. *et al.* Eukaryotic cell biology is temporally coordinated to support the energetic demands of protein homeostasis. *Nat. Commun.* **11**, (2020).

68. Lipton, J. O. *et al.* Aberrant Proteostasis of BMAL1 Underlies Circadian Abnormalities in a Paradigmatic mTOR-opathy. *Cell Rep.* **20**, 868–880 (2017).

69. Freedman, J. *Cell Physiology Source Book*. (Academic Press, 2012). doi:https://doi.org/10.1016/B978-0-12-387738-3.00001-9.

70. Choe, K. P. & Strange, K. Genome-wide RNAi screen and in vivo protein aggregation reporters identify degradation of damaged proteins as an essential hypertonic stress response. *Am. J. Physiol. - Cell Physiol.* **295**, (2008).

71. Stangherlin, A. *et al.* Compensatory ion transport buffers daily protein rhythms to regulate osmotic balance and cellular physiology. *bioRxiv* 2020.05.28.118398 (2020) doi:10.1101/2020.05.28.118398.

72. Pakos-Zebrucka, K. *et al.* The integrated stress response. *EMBO Rep.* **17**, 1374–1395 (2016).

73. Kroemer, G., Mariño, G. & Levine, B. Autophagy and the integrated stress response. *Mol. Cell*

40, 280–93 (2010).

74. Heifetz, A., Keenan, R. W. & Elbein, A. D. Mechanism of action of tunicamycin on the UDP-GlcNAc:dolichyl-phosphate GlcNAc-1-phosphate transferase. *Biochemistry* **18**, 2186–2192 (1979).

75. Oslowski, C. M. & Urano, F. Measuring ER stress and the unfolded protein response using mammalian tissue culture system. *Methods Enzymol.* **490**, 71–92 (2011).

76. Komar, A. A. & Merrick, W. C. A retrospective on EIF2A—and not the alpha subunit of EIF2. *International Journal of Molecular Sciences* vol. 21 (2020).

77. Schleich, S. *et al.* DENR-MCT-1 promotes translation re-initiation downstream of uORFs to control tissue growth. *Nature* **512**, 208–212 (2014).

78. Sendoel, A. *et al.* Translation from unconventional 5′ start sites drives tumour initiation. *Nature* **541**, 494–499 (2017).

79. Kim, J. H., Park, S. M., Park, J. H., Keum, S. J. & Jang, S. K. EIF2A mediates translation of hepatitis C viral mRNA under stress conditions. *EMBO J.* **30**, 2454–2464 (2011).

80. Xu, S. *et al.* Phospho-Tyr705 of STAT3 is a therapeutic target for sepsis through regulating inflammation and coagulation. *Cell Commun. Signal.* **18**, (2020).

81. Hu, D. *et al.* Essential role of IL-10/STAT3 in chronic stress-induced immune suppression. *Brain. Behav. Immun.* **36**, 118–127 (2014).

82. Yu, H., Pardoll, D. & Jove, R. STATs in cancer inflammation and immunity: A leading role for STAT3. *Nature Reviews Cancer* vol. 9 798–809 (2009).

83. Dibner, C. *et al.* Circadian gene expression is resilient to large fluctuations in overall transcription rates. *EMBO J.* **28262**, 123–134 (2009).

84. Putker, M. *et al.* Mammalian circadian period, but not phase and amplitude, is robust against redox and metabolic perturbations. *Antioxid. Redox Signal.* **4523**, ars.2016.6911 (2017).

85. Vecchi, G. *et al.* Proteome-wide observation of the phenomenon of life on the edge of solubility. *Proc. Natl. Acad. Sci. U. S. A.* **117**, 1015–1020 (2020).

86. Hipp, M. S., Kasturi, P. & Hartl, F. U. The proteostasis network and its decline in ageing. *Nat. Rev. Mol. Cell Biol.* **20**, 421–435 (2019).

87. Chan, A. B., Huber, A. L. & Lamia, K. A. Cryptochromes modulate E2F family transcription factors. *Sci. Rep.* **10**, (2020).

88. Huber, A. L. *et al.* CRY2 and FBXL3 Cooperatively Degrade c-MYC. *Mol. Cell* **64**, 774–789 (2016).

89. Liu, H. *et al.* The GID ubiquitin ligase complex is a regulator of AMPK activity and organismal lifespan. *Autophagy* **16**, 1618–1634 (2020).

90. Hoffmann, A. & Spengler, D. Chromatin remodeling complex NuRD in neurodevelopment and neurodevelopmental disorders. *Frontiers in Genetics* vol. 10 (2019).

91. Lombardi, L. M., Baker, S. A. & Zoghbi, H. Y. MECP2 disorders: From the clinic to mice and back. *Journal of Clinical Investigation* vol. 125 2914–2923 (2015).

92. Scheffner, M. & Kumar, S. Mammalian HECT ubiquitin-protein ligases: Biological and pathophysiological aspects. *Biochim. Biophys. Acta - Mol. Cell Res.* **1843**, 61–74 (2014).

93. Zhou, W., Wei, W. & Sun, Y. Genetically engineered mouse models for functional studies of SKP1-CUL1-F-box-protein (SCF) E3 ubiquitin ligases. *Cell Research* vol. 23 599–619 (2013).

94. Yerbury, J. J., Farrawell, N. E. & McAlary, L. Proteome Homeostasis Dysfunction: A Unifying Principle in ALS Pathogenesis. *Trends in Neurosciences* vol. 43 274–284 (2020).

95. Costa-Mattioli, M. & Walter, P. The integrated stress response: From mechanism to disease. *Science (New York, N.Y.)* vol. 368 (2020).

96. Hafycz, J. M. & Naidoo, N. N. Sleep, aging, and cellular health: Aged-related changes in sleep and protein homeostasis converge in neurodegenerative diseases. *Frontiers in Aging Neuroscience* vol. 11 (2019).

97. Hadizadeh Esfahani, A., Sverchkova, A., Saez-Rodriguez, J., Schuppert, A. A. & Brehme, M. A systematic atlas of chaperome deregulation topologies across the human cancer landscape. *PLoS Comput. Biol.* **14**, (2018).

98. Agyemang, A. F., Harrison, S. R., Siegel, R. M. & McDermott, M. F. Protein misfolding and dysregulated protein homeostasis in autoinflammatory diseases and beyond. *Seminars in Immunopathology* vol. 37 335–347 (2015).

99. Yalcin, A. & Hotamisligil, G. S. Impact of ER protein homeostasis on metabolism. *Diabetes* vol. 62 691–693 (2013).

100. Bur, I. M. *et al.* The circadian clock components CRY1 and CRY2 are necessary to sustain sex dimorphism in mouse liver metabolism. *J. Biol. Chem.* **284**, 9066–73 (2009).

101. Masuki, S., Todo, T., Nakano, Y., Okamura, H. & Nose, H. Reduced α-adrenoceptor responsiveness and enhanced baroreflex sensitivity in Cry-deficient mice lacking a biological clock. *J. Physiol.* **566**, 213–224 (2005).

102. Chan, A. B. & Lamia, K. A. Cancer, hear my battle CRY. *J. Pineal Res.* e12658 (2020) doi:10.1111/jpi.12658.

103. Kettner, N. M. *et al.* Circadian Homeostasis of Liver Metabolism Suppresses Hepatocarcinogenesis. *Cancer Cell* **30**, 909–924 (2016).

104. Lee, S., Donehower, L. A., Herron, A. J., Moore, D. D. & Fu, L. Disrupting Circadian Homeostasis of Sympathetic Signaling Promotes Tumor Development in Mice. *PLoS One* **5**, e10995 (2010).

105. Mteyrek, A. *et al.* Critical cholangiocarcinogenesis control by cryptochrome clock genes. *Int. J. Cancer* **140**, 2473–2483 (2017).

106. Cao, Q. *et al.* Circadian clock cryptochrome proteins regulate autoimmunity. *Proc. Natl. Acad. Sci. U. S. A.* **114**, 12548–12553 (2017).

107. Hand, L. E. *et al.* The circadian clock regulates inflammatory arthritis. *FASEB J.* **30**, 3759–3770 (2016).

108. Narasimamurthy, R. *et al.* Circadian clock protein cryptochrome regulates the expression of proinflammatory cytokines. *Proc. Natl. Acad. Sci. U. S. A.* **109**, 12662–12667 (2012).

109. Barclay, J. L. *et al.* High-fat diet-induced hyperinsulinemia and tissue-specific insulin

resistance in Cry-deficient mice. *AJP Endocrinol. Metab.* **304**, E1053–E1063 (2013).

110. Danziger, J. & Zeidel, M. L. Osmotic homeostasis. *Clin. J. Am. Soc. Nephrol.* **10**, 852–62 (2015).

111. Hoffmann, E. K., Lambert, I. H. & Pedersen, S. F. Physiology of Cell Volume Regulation in Vertebrates. *Physiol. Rev.* **89**, 193–277 (2009).

112. Dunlap, J. C. Molecular Bases for Circadian Clocks. *Cell* **96**, 271–290 (1999).

113. Wang, D. *et al.* A deep proteome and transcriptome abundance atlas of 29 healthy human tissues. *Mol. Syst. Biol.* **15**, (2019).

114. Shiber, A. *et al.* Cotranslational assembly of protein complexes in eukaryotes revealed by ribosome profiling. *Nature* **561**, 268–272 (2018).

115. Nangle, S. N. *et al.* Molecular assembly of the period-cryptochrome circadian transcriptional repressor complex. *Elife* **3**, e03674 (2014).

116. Jouffe, C. *et al.* The Circadian Clock Coordinates Ribosome Biogenesis. *PLoS Biol.* **11**, (2013).

117. Lamia, K. A. *et al.* Cryptochromes mediate rhythmic repression of the glucocorticoid receptor. *Nature* **480**, 552–556 (2011).

118. Vollmers, C. *et al.* Time of feeding and the intrinsic circadian clock drive rhythms in hepatic gene expression. *Proc. Natl. Acad. Sci.* **106**, 21453–21458 (2009).

119. Feltham, J. *et al.* Transcriptional changes are regulated by metabolic pathway dynamics but decoupled from protein levels. *bioRxiv* 833921 (2019) doi:10.1101/833921.

120. Ohtsuki, S. *et al.* Simultaneous absolute protein quantification of transporters, cytochromes P450, and UDP-glucuronosyltransferases as a novel approach for the characterization of individual human liver: Comparison with mRNA levels and activities. *Drug Metab. Dispos.* **40**, 83–92 (2012).

121. Cheng, Z. *et al.* Differential dynamics of the mammalian mRNA and protein expression response to misfolding stress . *Mol. Syst. Biol.* **12**, 855 (2016).

122. Zapalska-Sozoniuk, M., Chrobak, L., Kowalczyk, K. & Kankofer, M. Is it useful to use several

"omics" for obtaining valuable results? *Molecular Biology Reports* vol. 46 3597–3606 (2019).

123. Smith, J. R. & Whitney, R. G. Intraclonal variation in proliferative potential of human diploid fibroblasts: stochastic mechanism for cellular aging. *Science (80-.).* **207**, 82–84 (1980).

124. Phinney, D. G. Functional heterogeneity of mesenchymal stem cells: Implications for cell therapy. *Journal of Cellular Biochemistry* vol. 113 2806–2812 (2012).

125. Causton, H. C., Feeney, K. A., Ziegler, C. A. & O'Neill, J. S. Metabolic Cycles in Yeast Share Features Conserved among Circadian Rhythms. *Curr. Biol.* **25**, 1056–1062 (2015).

126. Yoo, S.-H. *et al.* PERIOD2::LUCIFERASE real-time reporting of circadian dynamics reveals persistent circadian oscillations in mouse peripheral tissues. *Proc. Natl. Acad. Sci. U. S. A.* **101**, 5339–46 (2004).

127. Seluanov, A., Vaidya, A. & Gorbunova, V. Establishing Primary Adult Fibroblast Cultures From Rodents. *J. Vis. Exp.* e2033–e2033 (2010) doi:10.3791/2033.

128. Plubell, D. L. *et al.* Extended Multiplexing of Tandem Mass Tags (TMT) Labeling Reveals Age and High Fat Diet Specific Proteome Changes in Mouse Epididymal Adipose Tissue. *Mol. Cell. Proteomics* **16**, 873–890 (2017).

129. Thaben, P. F. & Westermark, P. O. Detecting rhythms in time series with rain. *J. Biol. Rhythms* **29**, 391–400 (2014).

130. Eden, E., Navon, R., Steinfeld, I., Lipson, D. & Yakhini, Z. GOrilla: A tool for discovery and visualization of enriched GO terms in ranked gene lists. *BMC Bioinformatics* **10**, (2009).

131. Eden, E., Lipson, D., Yogev, S. & Yakhini, Z. Discovering motifs in ranked lists of DNA sequences. *PLoS Comput. Biol.* **3**, 0508–0522 (2007).

132. Deutsch, E. W. *et al.* The ProteomeXchange consortium in 2020: enabling 'big data' approaches in proteomics. *Nucleic Acids Res.* **48**, D1145–D1152 (2019).

133. Perez-Riverol, Y. *et al.* The PRIDE database and related tools and resources in 2019: improving support for quantification data. *Nucleic Acids Res.* **47**, D442–D450 (2018).

134. Feeney, K. A. *et al.* Daily magnesium fluxes regulate cellular timekeeping and energy balance.

Nature **532**, 375–379 (2016).

Figure legends

Figure 1: Cell-autonomous rhythms in the proteome and phosphoproteome persist in the absence of CRY. a) An overview of the proteomics experimental workflow. Samples were taken every 3 hours for 3 days in constant conditions, starting 24 h after medium change ("Experimental time 0 h"). **b), c)** Volcano plots showing the fold change in average expression of all proteins and phosphopeptides respectively, in CKO cells compared to WT (q = Benjamini-Hochberg corrected p-value, n= 24 time points over 3 days). Statistically significant changes ($q \leq 0.05$) are shown in red. Some proteins are labelled as space allows. **d), e)** Venn diagrams showing the numbers of rhythmic proteins and phosphopeptides respectively, in WT cells and CKO cells, with the overlaps annotated. Mean relative amplitude of rhythmic (phospho)peptides are also provided.

Figure 2: CRY regulates relative amplitude and phase of the rhythmic proteome and phosphoproteome. a) Fold-change in relative amplitude (RA) was calculated for each of the proteins found to be rhythmic in both genotypes by RAIN analysis (i.e. no RA cut-off). The mean fold change (log) in RA was an increase of 14% in CKO cells compared to WT cells (One sample t-test, $p<0.0001$). **b)** For each genotype, all proteins were divided into 10 deciles of equal number, ranked by abundance. The mean abundance of each decile was plotted against the proportion of the decile that was rhythmic. Linear regression lines are shown for each genotype, and the slopes were significantly non-zero (F test, WT $p=0.0016$, CKO $p<0.0001$). The slopes were also significantly different to each other (F test, $p=0.0001$). **c)** Fold-change in relative amplitude (RA) was calculated for each of the phosphopeptides found to be rhythmic in both genotypes by RAIN. On average, the RA was increased in CKO cells compared to WT cells by 6% (One sample t-test, $p<0.05$). **d)** The same analysis in b) was carried out for phosphopeptides. The slopes were significantly non-zero in CKO but not WT (F test, WT $p=0.3$, CKO $p=0.04$). The slopes were also significantly different to each other (F test, $p<0.0001$). **e, f)** Circular histograms showing the number of proteins at each rhythmic phase. Phase is defined and estimated by RAIN, as the time of the first predicted peak in a 24-hour period. Concentric circles

represent the counts scale, with the outermost circle marking the upper end of the counts. The distributions of rhythmic proteins in CKO cells were significantly different to WT cells (left, $p<0.001$, Watson's two-sample test). **g), h)** This was also the case for the proteins rhythmic in only one genotype (right, $p<0.001$, Watson's two-sample test). **i), j)** Circular histograms showing the number of phosphopeptides at each rhythmic phase. The distributions of rhythmic phosphopeptides in CKO cells was significantly different to WT cells ($p<0.001$, Watson's two-sample test).

Figure 3. CRYPTOCHROME regulates proteasome activity and translation rate.

a) From the quantitative proteomics experiment, average abundance of catalytic proteasome subunits was calculated and normalised to WT means. Trypsin-like (β2), chymotrypsin-like (β3) and caspase-like (β1) catalytic subunits are shown. The average was calculated from all 24 time points of the proteomics experiment. Mean±SD, 2-way ANOVA with Holm-Sidak's multiple comparisons. **b)** Representative Western blot using an antibody that recognises all 7 α subunits of the 20S proteasome, with anti-histone H3 as loading control. **c)** Quantification of the blots in b), using all replicates, normalised to WT mean. Mean±SD, one-tailed Student's t test with Welch correction – prior prediction from experiment in A) that CKO abundance would be lower. **d)** Proteasome activity measured using the ProteasomeGlo Assay (Promega), normalised to WT means. Mean±SD, 2-way ANOVA with Holm-Sidak's multiple comparisons. N=6 experiments, representative experiment shown (n=4 technical replicates). **e)** Translation rate was measured using ^{35}S-methionine labelling and imaging with phosphor screens. The quantification values were normalised to the total protein concentration as measured using Coomassie stain, and then normalised to WT mean. Mean±SD, Student's t test with Welch correction. N=3. **f)** Total protein mass per cell in confluent WT and CKO cultures. Cells were grown in two 12-well plates; one was used for cell counting and the other was used for lysis in RIPA buffer prior to protein quantification by BCA assay. Quantification shown, normalised to WT mean. Mean±SD, Student's t test with Welch correction.

Figure 4. Rhythmic regulation of ion transport in WT and CKO cells.

a) Gene ontology analysis for rhythmic proteins was carried out using Gene ontology enrichment analysis and visualisation (GOrilla) [130,131]. Significantly rhythmic WT proteins were compared against background (all proteins identified in the experiment), and the top non-overlapping GO Biological Process terms shown, sorted according to FDR q-value. Fold enrichment is annotated on each bar. The same GO analysis was carried out comparing proteins rhythmic that were rhythmic in CKO cells **(b)** and for proteins that were rhythmic across both genotypes **(c)**. **d), e)** From one time-course experiment, ions, cytosolic proteins and total protein were extracted in parallel samples. The presented experiment is representative of 3 separate time-course experiments that were carried out (N=3). Blue lines highlight the antiphasic relationship between oscillations in cytosolic protein and potassium concentration. Mean±SEM, p-values from RAIN, red lines are fits by a damped cosine compared with a straight line (null hypothesis). Parallel PER2::LUC recordings were also performed and plotted as a phase marker. **f)** Examples of key ion transporters are shown, as detected in the proteomics experiment. P values show the results of an F test comparing fits of damped cosine against straight line. All proteins except WT NKCC1 had RAIN p-values <0.05. **g), h)** Relative amplitudes of cytosolic protein and potassium concentrations oscillations in a) and b) were greater in CKO compared to WT (Student's t test with Welch correction, mean±SD).

Figure 5. CKO cells and tissues are more sensitive to stress.

a) WT and CKO cells were treated with 500 nM tunicamycin (TUN) and lysed in RIPA buffer at time points between 0-24 hours afterwards. Western blots were carried out, probing for phosphorylated eIF2α, total eIF2α and actin. Representative blots shown, n=4. **b)** Quantification of all replicates represented in (a), where phosphorylated eIF2α is normalised to total eIF2α. Mean±SD. 2-way ANOVA (TWA) with Holm-Sidak's multiple comparisons. **c)** Mouse lungs were collected 7 hours after transition to the light phase, 5 hours after intraperitoneal injection of mice with bortezomib (BTZ, 2.5 mg/kg) or vehicle (Veh, 1% DMSO in sterile PBS). Tissues were lysed in RIPA buffer and

1171 western blots were performed, probing for phosphorylated STAT3, total STAT3 and actin. All
1172 replicates shown, N=2 mice for each condition. **d)** Quantification of the blots shown in (c), where
1173 phosphorylated STAT3 is normalised to total STAT3. Mean±SD. 2-way ANOVA (TWA) with Holm-
1174 Sidak's multiple comparisons.
1175
1176 **Figure 6. WT cells recapitulate the CKO phenotype upon induced chronic stress.**
1177 **a)** WT PER2::LUC cells were treated with epoxomicin or vehicle control. Blue arrows show the time
1178 points where drug was washed off. Mean±SD. **b)** Quantification of damping rate of the PER2::LUC
1179 recordings shown in a), for the duration of drug treatment. Mean±SD. **c)** WT PER2::LUC cells were
1180 treated with tunicamycin or vehicle control. Mean±SD. **d)** Quantification of damping rate of the
1181 PER2::LUC recordings shown in c), for the duration of drug treatment. Mean±SD. **e)** WT
1182 PER2::LUC cells were treated with radicicol or vehicle control. Blue arrows show the time points
1183 where drug was washed off. Mean±SD. **f)** Quantification of damping rate of the PER2::LUC
1184 recordings shown in e), for the duration of drug treatment. Mean±SD. **g)** Schematic diagram:
1185 altogether our data suggests that in the absence of CRY, proteome imbalance disrupts circadian
1186 rhythmicity of physiology. See text for details.
1187

FIGURE 1

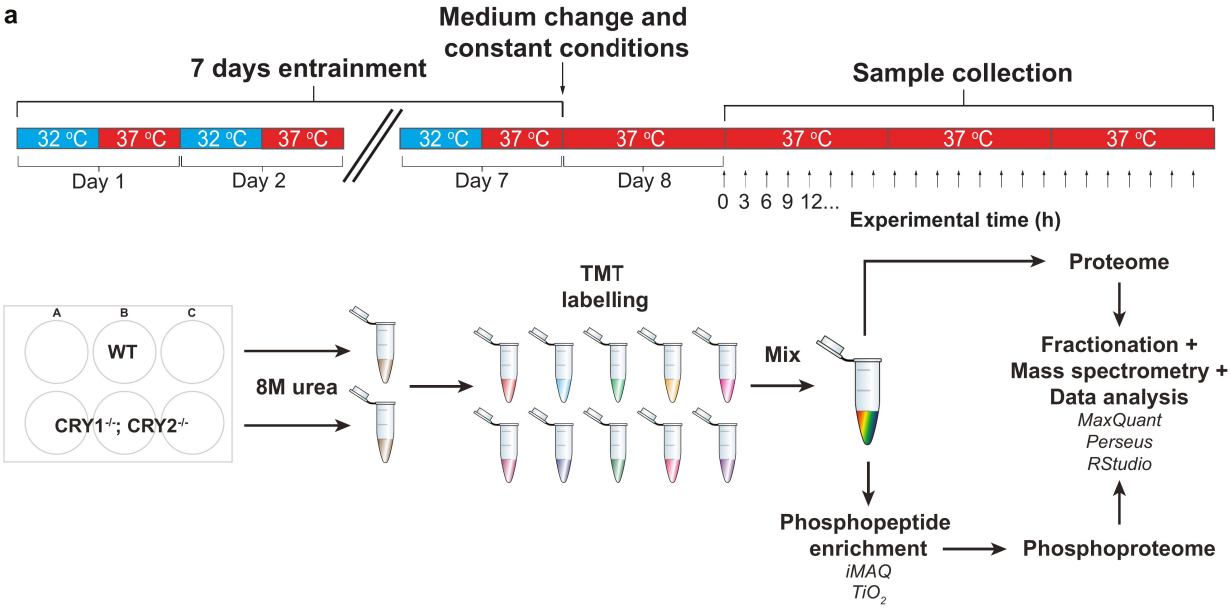

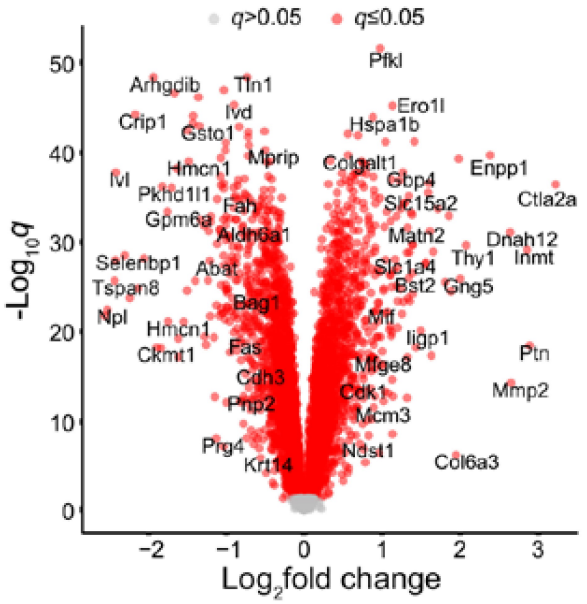

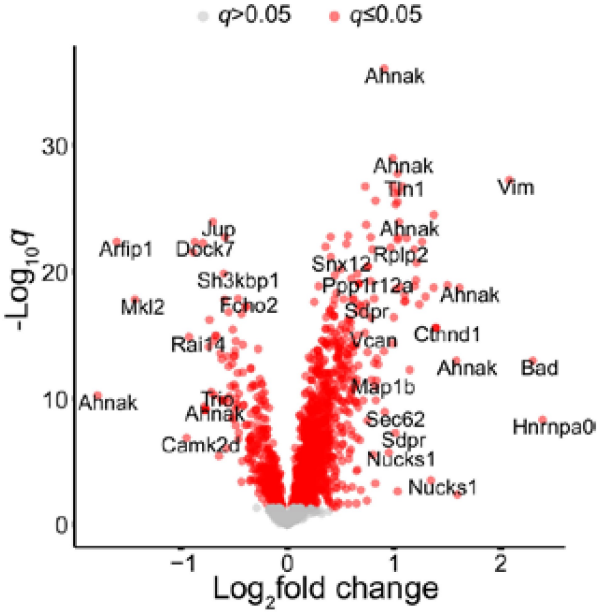

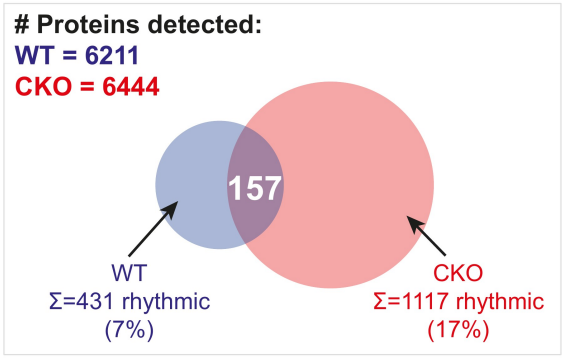

Relative amplitudes:
WT mean = 18%
CKO mean = 18%

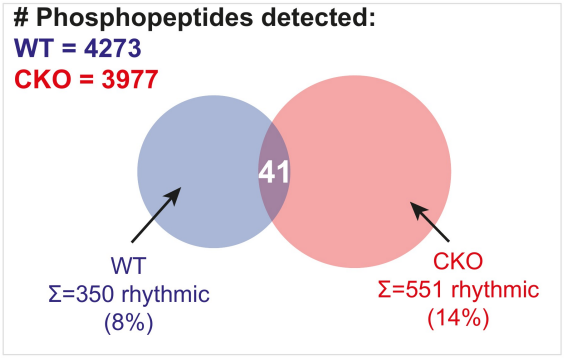

Relative amplitudes:
WT mean = 29%
CKO mean = 32%

FIGURE 2

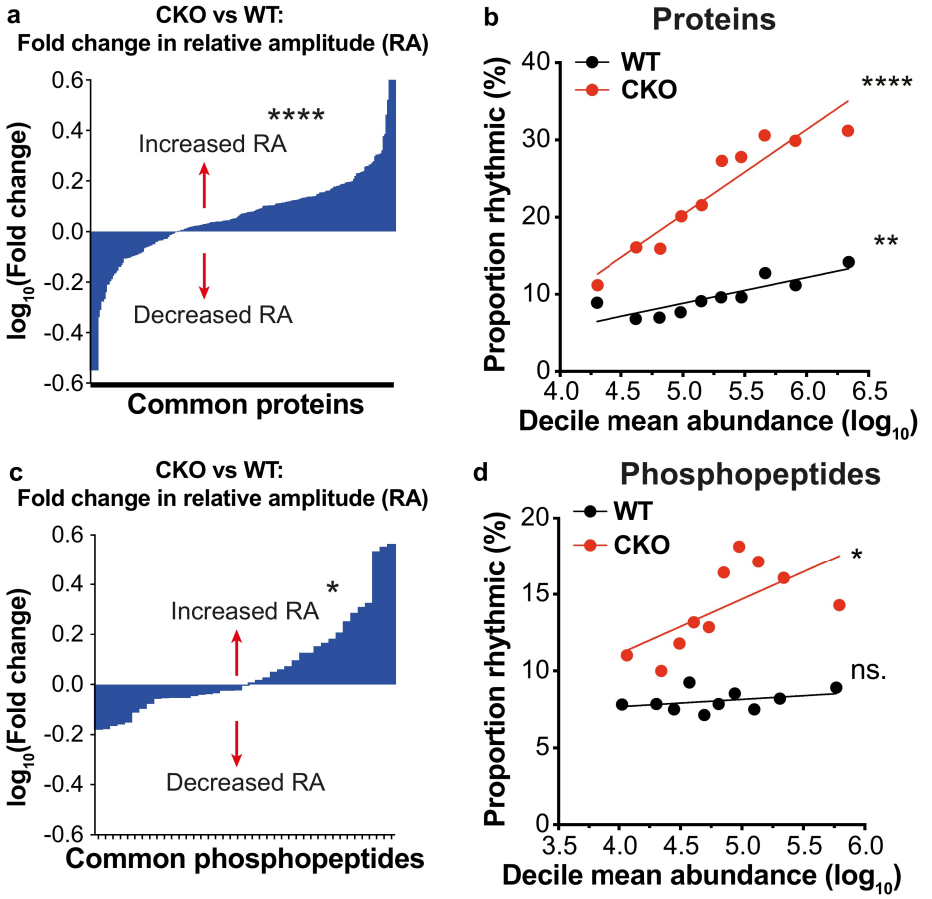

FIGURE 3

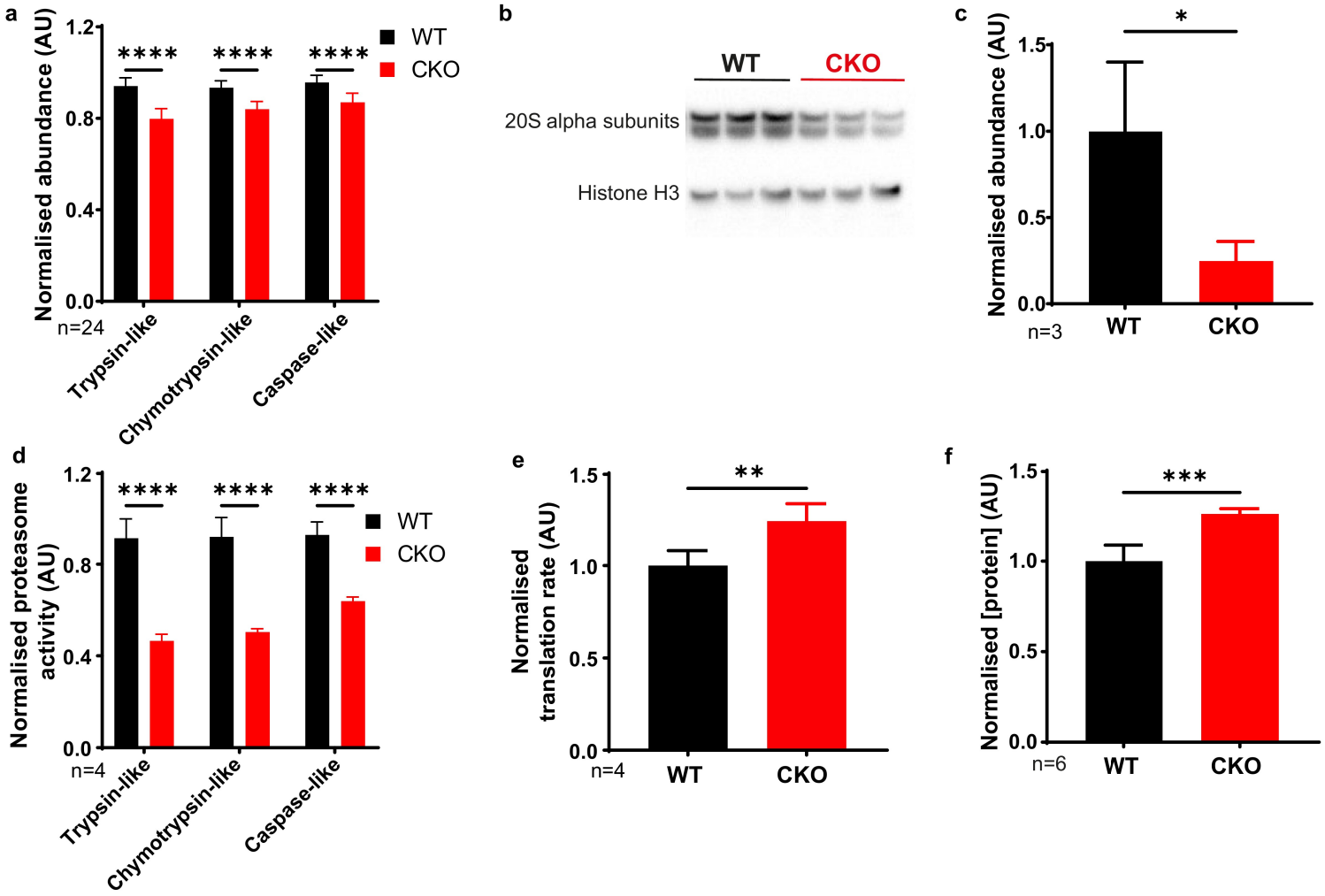

FIGURE 4

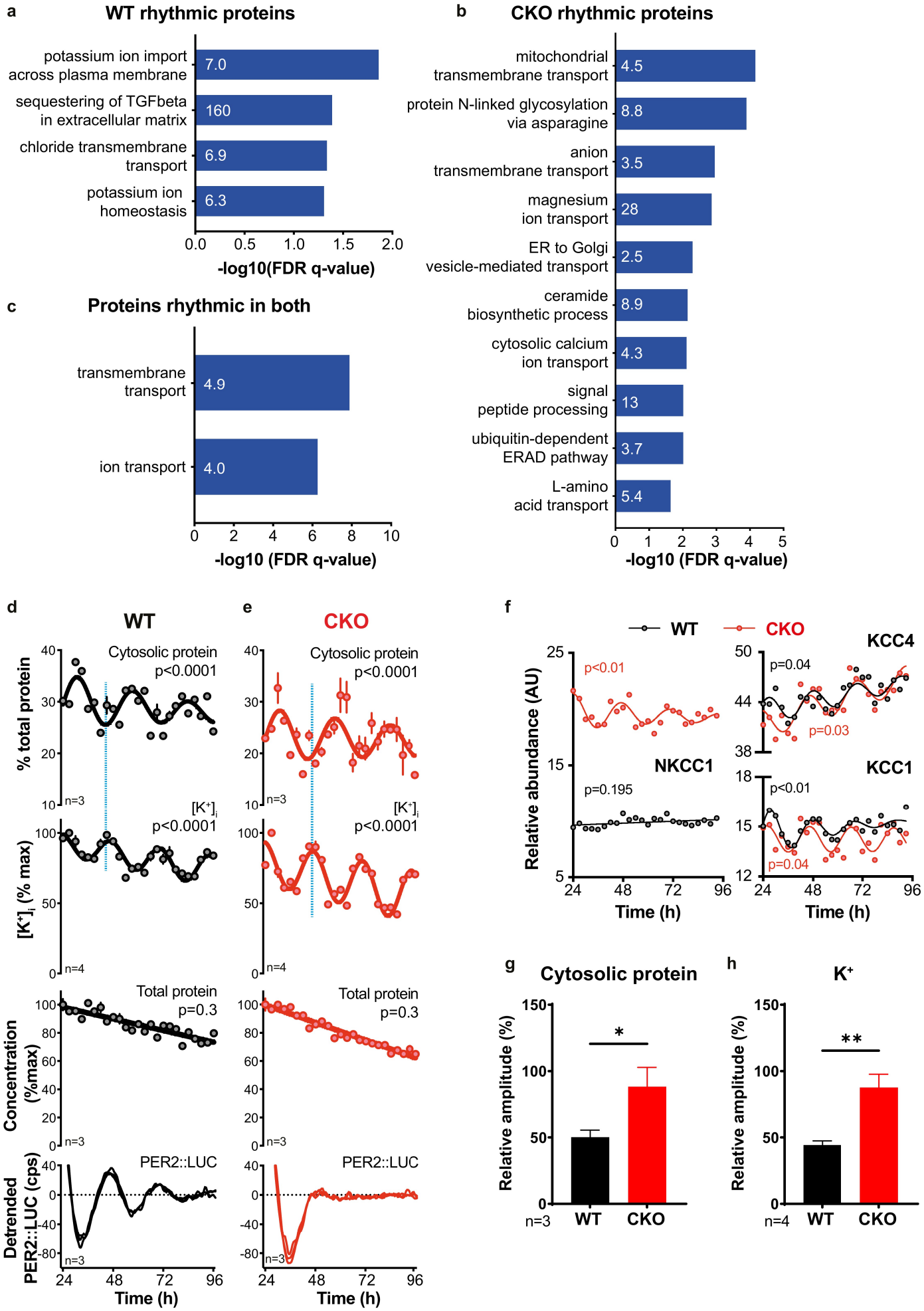

FIGURE 5

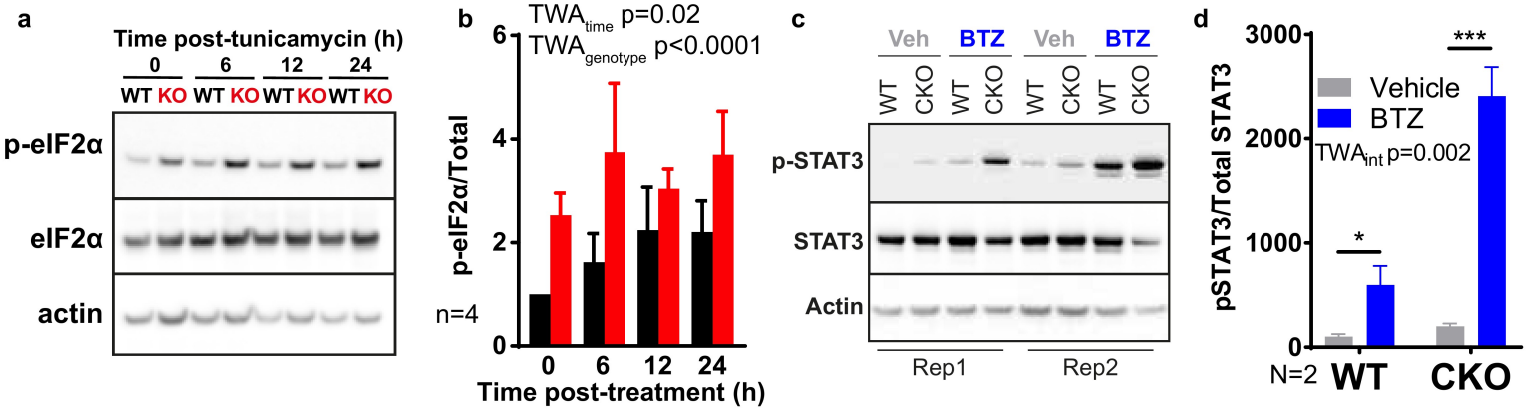

FIGURE 6